TRENDS IN SCIENCES 2026; 23(4): 10899
https://doi.org/10.48048/tis.2026.10899 RESEARCH ARTICLE

Biflavonoids from Araucaria Genus as Selective PDE4 Inhibitors: Insights from *In Silico* and *In Vitro* Studies

Nafisah[1], Budi Arifin[2], Setyanto Tri Wahyudi[3], Uus Saepuloh[4], Kurniawanti[2], Silmi Mariya[4] and Purwantiningsih Sugita[2,*]

[1]*Postgraduate Chemistry Student of Postgraduate School, IPB University, Bogor 16680, Indonesia*
[2]*Department of Chemistry, Faculty of Mathematics and Sciences, IPB University, Bogor 16680, Indonesia*
[3]*Department of Physics, Faculty of Science, IPB University, Bogor 16680, Indonesia*
[4]*Primate Research Centre, IPB University, Bogor 16151, Indonesia*

([*]Corresponding author's e-mail: purwantiningsih@apps.ipb.ac.id)

Received: 9 June 2025, Revised: 28 July 2025, Accepted: 4 August 2025, Published: 25 December 2025

Abstract

Chronic inflammation is a major contributor to autoimmune diseases, necessitating the discovery of selective phosphodiesterase-4 (PDE4) inhibitors. Biflavonoids, with diverse biological activities, exhibit anti-inflammatory potential. This study employed molecular docking and molecular dynamics (MD) simulations to evaluate the interaction of 25 biflavonoid compounds with PDE4B and PDE4D. The most promising compound was validated using *in vitro* enzyme inhibition assays. Molecular docking identified 7,7"-di-*O*-methylamentoflavone as a potent PDE4B inhibitor with strong binding affinity and favourable MM/GBSA binding energy of –49.56 ± 4.12 kcal/mol, compared to its PDE4D binding energy of –39.77 ± 5.21 kcal/mol. Molecular dynamics simulations confirmed the stability of ligand–protein interactions. *In vitro* assays of six isolated biflavonoids from *Araucaria hunsteinii* and *Araucaria cunninghamii* confirmed that 7,7"-di-*O*-methylamentoflavone as a selective PDE4B inhibitor, with an IC_{50} value of 13.9 ± 2.38 µM. This study provides new insights into the potential of biflavonoids as selective PDE4B inhibitors. However, further research is required to validate their therapeutic potential, including *in vivo* evaluation and broader safety profiling.

Keywords: Anti-inflammatory, Biflavonoids, Enzyme inhibition, Molecular docking, Molecular dynamics, PDE4 inhibitors

Introduction

Chronic inflammation is a critical driver of numerous diseases, including chronic obstructive pulmonary disease (COPD), asthma, arthritis and cancer [1]. While a controlled inflammatory response is essential for eradicating pathogens, excessive or prolonged inflammation can damage host tissues and contribute to the progression of degenerative diseases. Consequently, targeting inflammation through effective therapeutic strategies has become a priority in medical research [2]. Phosphodiesterase (PDE) is an intracellular enzyme that plays a role in catalyzing the hydrolysis of cyclic guanosine monophosphate (cGMP) and cyclic adenosine monophosphate (cAMP). These two molecules function as second messengers in signal transduction and regulate various physiological processes, such as visual transduction, cell proliferation and differentiation, cell cycle regulation, gene expression, inflammation, apoptosis and metabolic functions [3]. Phosphodiesterase-4 (PDE4), a key enzyme that regulates inflammatory responses, has emerged as a promising target for the development of anti-inflammatory drugs. PDE4 is predominantly expressed in immune and inflammatory cells, modulating cyclic adenosine monophosphate (cAMP) levels. Inhibiting PDE4 has been shown to suppress a wide spectrum of inflammatory responses both *in vitro* and *in vivo* [4]. Although PDE4 inhibitors are effective

anti-inflammatory agents, their clinical use is limited by adverse effects such as nausea and emesis, primarily attributed to PDE4D inhibition. Thus, isoform-selective inhibition, particularly toward PDE4B, is highly desirable [5]. As a result, there is a growing interest in developing selective PDE4B inhibitors to achieve therapeutic efficacy with fewer side effects.

Over the past four decades, significant advancements have been made in identifying PDE4 inhibitors as therapeutic agents. This has resulted in a comprehensive collection of preclinical and clinical data that strongly supports drug discovery efforts for new treatments of inflammatory diseases such as COPD, asthma and psoriasis. During this process, many agents with diverse structures have been developed and evaluated pharmacologically, revealing, in some cases, promising therapeutic potential. However, only a few PDE4 inhibitors have been approved as medications. This is primarily due to the adverse effects observed with several PDE4 inhibitors under development, which were initially linked to a lack of specificity in their mechanism of action, hindering their full clinical development. One significant challenge that underscores the complexity of our task is the difficulty in creating isoform-selective PDE4 inhibitors, owing to the high degree of sequence and structural similarity between the various subtypes, especially in conserved regions of the catalytic site [6]. In this context, the identification of new molecules as isoform-selective PDE4 inhibitors continues to be an active field of investigation within drug discovery.

The production of pro-inflammatory cytokines and inflammatory cytokines is regulated via the degradation of cAMP by PDE4 (**Figure 1**). The inhibition of PDE4 results in the elevation of cAMP level and activation of PKA and exchange protein directly activated by cAMP (Epca 1/2). The activation of PKA leads to the phosphorylation of cAMP-responsive element-binding protein (CREB) and activation of the transcription factor 1 (ATF-1) which results in increasing the production of anti-inflammatory cytokines and decreasing the inflammatory cytokines [7,4]. Rolipram, a first-generation selective PDE4 inhibitor, was investigated for asthma treatment but was limited by gastrointestinal and CNS side effects. Roflumilast, the only PDE4 inhibitor approved by the FDA, is used for COPD but has limited efficacy in acute bronchoconstriction [6,8]. Several biflavonoid compounds such as amentoflavone, podocarpusflavone A, sequoiaflavone, podocarpusflavone B and 7,7″-di-*O*-methylamentoflavone showed strong inhibitory activity against various PDE isoforms. 7,7″-di-*O*-methylamentoflavone has been identified as a selective PDE4 inhibitor (IC_{50} = 1.48 ± 0.21 μM), showing comparable activity to rolipram and making it a promising lead scaffold for drug development [9]. This natural compound appears to be a strong and selective PDE4 inhibitor, making it a promising candidate for further exploration in the development of new treatments for chronic obstructive pulmonary disease and asthma with minimal side effects.

Ligand-based pharmacophore models for diverse classes of PDE4B and PDE4D inhibitors were developed by [10]. Hydrogen bond acceptors were identified to be mainly responsible for PDE4B inhibition, while both hydrogen bond acceptors and hydrophobic groups were found to be responsible for PDE4D inhibition. In another study, six compounds from the result of ligand-based pharmacophore modelling showed higher PDE4B inhibitory activity (2 - 461 nM) than the rolipram [11]. The similarity between the biflavonoid and the reported PDE4 inhibitors (rolipram and roflumilast) (**Figure 1**) is that they all have an aromatic ring (benzene or heterocyclic systems) and oxygen-containing functional groups (OH, OCH_3, carbonyl), which contribute to their stability and biological activity. Thus, we chose biflavonoids to be the target of this research.

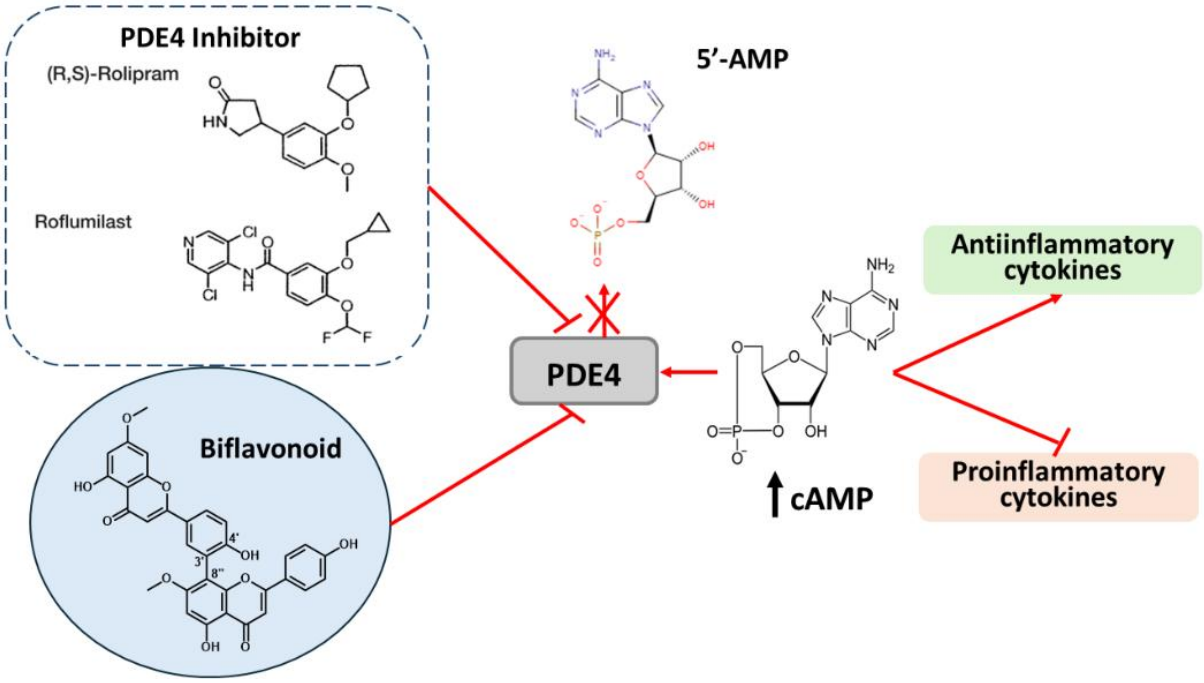

Figure 1 A brief schema of PDE4 in the regulation of inflammatory response.

Biflavonoids are polyphenolic compounds composed of two identical or distinct flavonoid units linked symmetrically or asymmetrically through C-C or C-O-C linkers [12]. Their anti-inflammatory properties have been extensively studied at the molecular level. Specific biflavonoid compounds, such as moreloflavones [13], amentoflavone [14], ginkgetin with an IC_{50} of 0.75 μM [15] and ochnaflavones [16], have demonstrated the ability to inhibit pro-inflammatory enzymes like phospholipase A2 (PLA2) and cyclooxygenase (COX), although challenges remain regarding their bioavailability [17]. Among these, 7,7"-di-*O*-methyllamentoflavone has been identified as a selective inhibitor of PDE4 and a promising anti-inflammatory agent, with an IC_{50} of 1.48 ± 0.21 μM [9]. In addition to their anti-inflammatory effects, biflavonoids exhibit a wide range of biological activities, including antiviral [18-19], anti-osteoporosis [20], antiplasmodium [21], antioxidants [22], antibacterial [23], and anticancer [24] properties. Biflavonoids have been extensively studied over the past 30 years and identified in numerous plant species. Notably, the genus *Araucaria*, a member of the Araucariaceae family, is known to produce significant secondary metabolites, including biflavonoids and terpenoids [25]. Biflavonoids of the Araucariaceae family significantly modulate key inflammatory pathways, including cytokine suppression and NF-κB inhibition [26]. Several *Araucaria* species have been reported as sources of biflavonoids, such as *A. excelsa and A. cookii* from India [27], *A. araucana* from India [28], Brazil pine (*A. angustifolia*) [29], pine *hoop* (*A. cunninghamii*) [23,24], *A. bidwilii* from Egypt [32], *A. columnaris* from India [33], *A. hunsteinii* K. Schum from Indonesia [13, 18] and *A. columnaris* from Indonesia [34].

In recent years, *in silico* approaches have become essential in drug discovery, enabling the efficient identification of new therapeutic compounds. These computational methods play a critical role in the modern pharmaceutical industry by reducing the time and resources required for drug development. This study focuses on identifying biflavonoids with strong anti-inflammatory potential by evaluating 25 biflavonoid derivatives from Genus *Araucaria* reported by [35]. These biflavonoid derivatives were selected for docking because they fulfil the requirements for an orally active drug, according to Lipinski's rule of five and of the ADMET prediction study, compared to their basic skeletal biflavonoids such as amentoflavone, cupresuflavone, agathisflavone and robustaflavone [35]. Previous research has explored the anti-inflammatory properties of *Araucaria* species [26]. For example, studies on the polyphenol-rich fraction of *Araucaria*

bidwillii demonstrated significant anti-inflammatory activity [32], while other work has examined the antioxidant and anti-inflammatory potential of three *Araucaria* species [36]. Despite these advancements, the specific potential of biflavonoid compounds from the genus *Araucaria* as anti-inflammatory agents, particularly in terms of inhibiting PDE4 enzymes, remains unexplored. This study aims to address this gap by combining *in silico* and *in vitro* approaches to investigate the inhibitory activity of biflavonoid compounds from the genus *Araucaria* against PDE4B and PDE4D enzymes so that it can be a reference for understanding the molecular mechanism of flavonoids as PDE4 inhibitors and open up new opportunities in the treatment of inflammatory diseases with minimal side effects. This study contributes to the limited number of investigations exploring Indonesian *Araucaria*-derived biflavonoids as PDE4 inhibitors using a combined *in silico* and *in vitro* approach. This study adopts a sequential *in silico–in vitro* workflow to efficiently identify PDE4 inhibitors from Araucaria-derived biflavonoids. Computational screening guided compound selection for *in vitro* validation, offering mechanistic insights into PDE4 isoform selectivity and laying the groundwork for future *in vivo* and preclinical investigations.

To strengthen the efficiency and direction of compound selection, this study employs a sequential *in silico-in vitro* approach to enhance the efficiency of early PDE4 inhibitor discovery. *In silico* screening, using docking and molecular dynamics simulations, enabled the identification of potential biflavonoids with high predicted affinity and selectivity for PDE4B. These computational predictions led to the prioritisation of compounds for *in vitro* validation, thereby reducing the experimental burden and providing mechanistic insights into ligand-enzyme interactions. This comprehensive approach exemplifies a sensible and resource-efficient strategy for discovering selective anti-inflammatory drugs.

Materials and methods

Materials

The materials used for computational research were 25 biflavonoid compounds that had been isolated from the genus *Araucaria* based on the literature review [26], 3-D crystal structures of target proteins PDE4B (Q07343) and PDE4D (Q08499) obtained through PDB from Uniprot data. Three pure isolates of biflavonoids from *A. cunninghamii*, namely 4',4"',7,7"'-tetra-*O*-methylcuprasoflavone, 7,4",4"'-tri-*O*-methylrobustaflavone, and 7,7"-di-*O*-methylamentoflavone in the previous report [37], three compounds from *A. hunsteinii*, namely 4',7,7"-tri-*O*-methylcuprasoflavone, 4",7,7"-tri-*O*-methylagatisflavone and 7,4"'-di-*O*-methylcuprasoflavone in the previous report [24] from Bogor Botanical Garden (Indonesia), PDE4B (No. FY-EH23197) and PDE4D (No. FY-EH9346) ELISA kits from Feiyue Biotechnology, Michigan cancer foundation-7 (MCF-7) cells (ATCC HTB 22), phosphate-buffered saline (PBS), trypsin, MCF-7 cell growth media (Roswell park memorial institute (RPMI) 1640 and fetal bovine serum (FBS)), and a mixture of antibiotics (penicillin and streptomycin).

Preparation of receptor target, test ligand co-crystal ligand

The test ligands, which comprised 25 biflavonoid compounds from the genus Araucaria (Table 1), were first created as two-dimensional (2D) structures using the ChemDraw Ultra 12 program. Comparison ligands, including roflumilast, rolipram and cyclic adenosine monophosphate (cAMP), were also prepared. The 2D structures were then converted into three-dimensional (3D) models using Chem3D and saved in *.pdb format. Geometry optimization and energy minimization of molecular structures were carried out using molecular mechanics methods using the Open Babel program with the Steepest Descent and Newton-Raphson methods and the GAFF (General Amber Force Field) force field. The test and comparison ligands were processed using AutoDock Tools 1.5.7 through a command line in Linux. This processing included adding hydrogen atoms, merging non-polar hydrogens, assigning Gasteiger charges and defining the number of active torsions. The modified files were subsequently saved in *.pdbqt format, following the modifications described by [38].

Table 1 Test ligan of biflavonoid compounds from the genus *Araucaria*.

Structure	R_1 (*7*)	R_2 (*4′*)	R_3 (*7″*)	R_4 (*4‴*)	Compound name	No
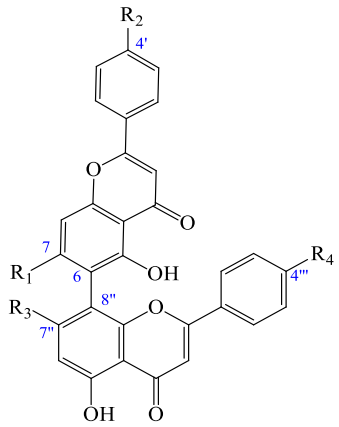	OH	OH	OCH_3	OH	7"-*O*-methylagathisflavone	1
	OCH_3	OH	OCH_3	OH	7,7″-di-*O*-methylagathisflavone	2
	OCH_3	OH	OH	OCH_3	7,4‴-di-*O*-methylagathisflavone	3
	OCH_3	OH	OH	OH	7-*O*-methylagathisflavone	4
	OCH_3	OH	OCH_3	OCH_3	7,4‴,7″-tri-*O*-methylagathisflavone	5
	OCH_3	OCH_3	OCH_3	OH	7,4′,7″-tri-*O*-methylagathisflavone	6
	OCH_3	OCH_3	OCH_3	OCH_3	7,4′,7″,4‴-tetra-*O*-methylagathisflavone	7
	OH	OCH_3	OCH_3	OH	4′,7″-di-*O*-methylagathisflavone	8
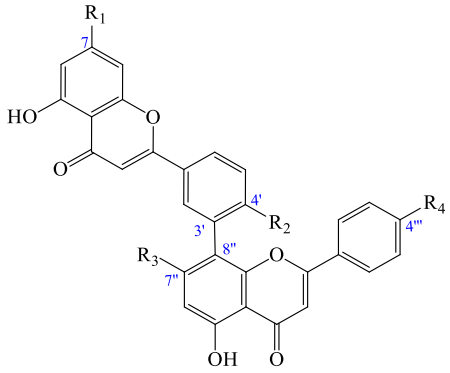	OCH_3	OCH_3	OCH_3	OH	7,4′,7″-tri-*O*-methylamentoflavone	9
	OCH_3	OCH_3	OH	OCH_3	7,4′,4‴-tri-*O*-methylamentoflavone	10
	OH	OCH_3	OH	OCH_3	4′,4‴-di-*O*-methylamentoflavone	11
	OH	OH	OCH_3	OH	7″-*O*- metilamentoflavone	12
	OCH_3	OH	OCH_3	OH	7,7″-di-*O*-methylamentoflavone	13
	OCH_3	OCH_3	OCH_3	OCH_3	7,4′,7″,4‴-tetra-*O*-methylamentoflavone	14
	OCH_3	OCH_3	OH	OH	7,4′-di-*O*-methylamentoflavone	15
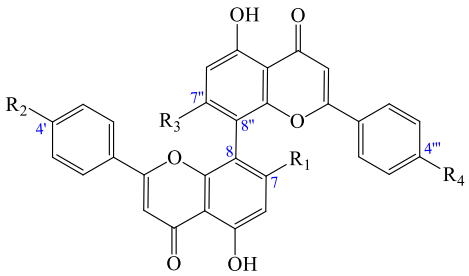	OCH_3	OH	OH	OH	7-*O*-methylcupressuflavone	16
	OCH_3	OH	OCH_3	OH	7,7″-di-*O*-methylcupressuflavone	17
	OCH_3	OCH_3	OCH_3	OH	7,4′,7″-tri-*O*-methylcupressuflavone	18
	OH	OCH_3	OH	OCH_3	4′,4‴-di-*O*-methylcupressuflavone	19
	OCH_3	OCH_3	OCH_3	OCH_3	7,4′,7″,4‴-tetra-*O*-methylcupressuflavone	20
	OCH_3	OH	OCH_3	OCH_3	7,7″,4‴-tri-*O*-methylcupressuflavone	21
	OCH_3	OH	OH	OCH_3	7,4‴-di-*O*-methylcupressuflavone	22

Structure	R_1 (*7*)	R_2 (*4′*)	R_3 (*7″*)	R_4 (*4‴*)	Compound name	No
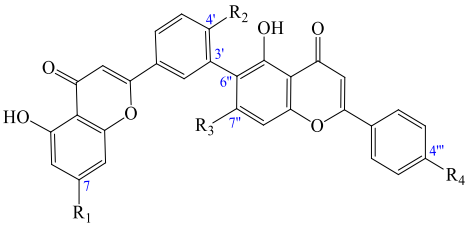	OH	OH	OCH_3	OH	7"-*O*-methylrobustaflavone	23
	OCH_3	OCH_3	OCH_3	OH	7,4',7"-di-*O*-methylrobustaflavone / Imbricataflavone A	24
	OCH_3	OCH_3	OH	OCH_3	7,4',4"'-tri-*O*-methylrobustaflavone	25

The target enzymes PDE4B and PDE4D in humans were accessed via UniProt (www.uniprot.org) and ten wild-type structures for each enzyme were selected based on a resolution of less than 2.5 Å and Ramachandran plot analysis. These structures were downloaded in *.pdb format from the RCSB Protein Data Bank (PDB). The receptor files were prepared using AutoDock Tools, employing a command-line workflow that involved removing water molecules, adding Gasteiger charges and associating hydrogen atoms. The processed receptor files were then saved in *.pdbqt format for docking studies [39].

Molecular docking simulation

The self-docking method was validated using AutoDock Vina software executed via the command line. This involved docking the co-crystal ligand with the receptor protein, generating multiple ligand poses. From these, the pose with the smallest root-mean-square deviation (RMSD) value was selected as the optimal reference pose for further analysis. A cross-docking procedure was then performed to evaluate 25 test ligands, along with reference ligands cyclic adenosine monophosphate (CMP), roflumilast (ROF) and rolipram (ROL) against the receptor proteins. AutoDock Vina software was employed for this process, with each docking simulation repeated ten times to ensure consistency. Molecular docking was performed using AutoDock Vina with the following parameters: Grid spacing of 1 Å, grid box dimensions of 20×20×20 $Å^3$ and exhaustiveness set to 32. A total of 10 output poses were generated per ligand. The random seed was left at its default value, allowing variation between runs. The grid centre were determined based on the optimal results from the self-docking validation (detailed information of the AutoDock Vina command-line input and configuration files in SI). The docking simulations yielded binding energy values (kcal/mol), which were analyzed to assess ligand-receptor interactions. These interactions, including hydrophobic bonds and hydrogen bonds, were visualized using Pymol 3.1.4 and LigPlot+ software. Ligands were ranked based on their binding energy values and their selectivity for PDE4B over PDE4D. The test ligand with the most negative (i.e., most favourable) binding energy for PDE4B was identified as the best candidate. Reference ligands such as ROL, CMP and ROF served as benchmarks to evaluate the affinity and selectivity of the test ligands, providing a comparative framework for the docking results.

Molecular dynamics simulation

Selected protein-ligand complexes were prepared using the AMBER20 program. Water and hydrogen were removed from the complex using Pdb4amber. Next, the pK value of the ionized group on the amino acid residue was calculated using the H^{++} website (http://biophysics.cs.vt.edu/) at pH 7.0. The program H^{++} can predict the amino acid with a non-standard protonation state and adds missing hydrogen atoms according to the specified pH of the environment. The ligand-receptor complex molecules are each given an AMBER ff14sb force field. In the periodic boundary conditions (PBC), the system was dissolved with TIP-3P water molecules with a gap of 1.0 nm and neutralised using Na^+/Cl^-. In the heating stage, amino acid residues are limited by 10 kcal/mol with the NVT ensemble (constant number of particles, volume and temperature). The system is heated until it reaches a temperature of 312 K. In the equilibration stage, the heating limitation is released gradually. The production simulation process uses PMEMD.CUDA, to see the free movement of molecules without restrictions for 100 ns at a fixed temperature of 312 K. Evaluation of structural

properties, root mean square deviation (RMSD) of the complex and determination of the hydrogen bonds are carried out using CPPTRAJ module from AmberTools. The relative free energy of binding was calculated using the Molecular Mechanics Generalized Born Surface area (MM/GBSA) method [40].

For calculation MM/GBSA of the gas-phase interaction energy (ΔE_{MM}) and the non-polar part (ΔG_{SA}) of the solvation energy and the electrostatic solvation energy (ΔG_{GB}), 50,000 frames evenly extracted from a single MD trajectory of the complex from 0 to 100 ns were used, using the GB model with parameters igb = 2, which generally represents air conditions implicitly, a salt concentration of 0.100 M to represent the physiological environment and using a probe radius of 1.4 Å, which represents the size of air molecules when calculating the solute surface. Binding free energy (ΔGbind) between a ligand (L) and a receptor (R) to form a complex RL is calculated as [41]:

$$\Delta G_{bind} = \Delta H - T\Delta S \approx \Delta E_{MM} + \Delta G_{sol} - T\Delta S \quad (1)$$

$$\Delta E_{MM} = \Delta E_{internal} + \Delta E_{electrostatic} + \Delta E_{electrostatic} \quad (2)$$

$$\Delta G_{sol} = \Delta G_{GB} + \Delta G_{SA} \quad (3)$$

***In vitro* PDE4B and PDE4D inhibition assay**

MCF-7 cells were grown in 24-well microplates with a concentration of 5,000 cells in 100 µL of growth medium (D-MEM, RPMI 1,640 and FBS 5%) and antibiotic mixtures (penicillin 100 U/mL and streptomycin 100 mg/mL). To assess PDE4B and PDE4D enzyme inhibition in MCF-7 cells, we utilised a direct cAMP ELISA-based assay (Feiyue Biotechnology) following cell lysis after compound treatment. Since PDE4 enzymes hydrolyse cAMP, inhibition leads to intracellular cAMP accumulation, which is quantitatively measured as the primary readout. The resulting IC_{50} values reflect the concentration required for 50% inhibition of PDE4B or PDE4D enzymatic activity. To distinguish PDE4B and PDE4D inhibition, separate ELISA kits with isoform-specific antibodies were used for each enzyme target. Pure isolates of compounds 5, 18 and 22 from *A. hunsteinii* K. Schum leaves and compounds 13, 20 and 26 from *A. cunninghamii* leaves were each added after the cells reached 50% confluency (24 h) and a negative control was prepared. All of the samples and controls were carried out with three replicates [42]. Cells are gently washed with cold phosphate-buffered saline (PBS) in moderate amounts and released with trypsin. Cells are centrifuged for 5 min at 1,000×g (suspension cells can be collected by centrifugation directly). The supernatant is discarded and the cells are washed 3 times with cold PBS. Cells are diluted in cold PBS until they amount to 5×106 cells/mL. The freeze-thaw process is repeated several times until the cells are fully lysed, then centrifuged for 10 min at 1,500×g at 2 - 8 °C. The cell lysates are either tested immediately or stored at –20 or –80 °C for later use.

The cell lysates were collected following centrifuging for 5 min at 600×g and then determined by the direct cAMP PDE4B and PDE4D ELISA kit (Feiyue Biotechnology, Wuhan, China) according to the manufacturer's instruction. Absorbances are read at a wavelength of 450 nm (OD450) using Microplate Reader S/N 11421. The IC_{50} values were determined by nonlinear regression analysis and a sigmoidal dose-response equation using GraphPad Prism 4 (GraphPad Software Inc., La Jolla, CA, USA) [43].

The MCF-7 cell line was chosen because of its well-characterised cAMP–PKA signalling pathway and modest endogenous production of PDE4 isoforms. Despite being extensively employed in breast cancer research, MCF-7 is appropriate for assessing PDE4 inhibition due to its functional susceptibility to intracellular cAMP modulation. MCF-7 offers a human-derived epithelial model that circumvents the immunological-related variables and variability found in primary immune cells. PDE4B and PDE4D activities were evaluated using their basal expression levels in MCF-7 cells; no inflammatory stimulation was used in this assay.

Results and discussion

Protein structures and validation parameters

Docking simulations involving PDE4B and PDE4D receptors with 25 test ligands of biflavonoid compounds from the genus *Araucaria*. The 3-D structures of PDE4B and PDE4D proteins obtained from the UniProt and Protein Data Bank sites consist of 40 and 103 protein structures, respectively. Ten selected wildtype structures from each receptor used in this study

(**Table 2**) were based on parameter resolution values ≤ 2.5 Å, most favoured regions value above 90% and positive G-factors values. A resolution value of ≤ 2.5 Å determines that the docking process runs well [44]. Based on the Ramachandran plot, a good quality model is expected to have more than 90% in the most favoured regions [45]. The G-factor is a value that measures the stereochemistry of a protein model. A low G-factor value indicates the protein model has a low conformational probability. The ideal G-factor value is above –0.5 [46]. The self-docking results in the form of RMSD values are shown in **Table 2**. A smaller RMSD value (closer to 0) indicates the docked ligand pose's similarity with the experiment's co-crystal ligand.

Table 2 List of protein structures and RMSD values from self-docking results.

No	PDB ID	Resolution (Å)	Plot ramachandran analysis		RMSD (Å)	Ligand ID
			Most favoured regions (%)	G-Factors		
PDE4B *wild type*						
1	4KP6	1.50	92.8	0.28	6.32	1S1
2	5OHJ	1.60	91.8	0.07	0.36	9VE
3	4MYQ	1.90	93.2	0.20	1.15	19T
4	2CHM	1.60	94.1	0.50	1.99	3P4
5	2QYL	1.90	92.1	0.47	0.36	NPV
6	1TB5	1.90	92.2	0.22	5.67	AMP
7	4NW7	1.90	93.2	0.13	0.47	2O5
8	1XMU	1.90	90.6	0.28	1.54	ROF
9	1XN0	2.31	90.4	0.24	0.77	ROL
10	3WD9	2.50	92.4	0.13	0.49	QCP
PDE4D *wild type*						
1	1Y2B	1.40	93.40	0.41	3.16	DEE
2	6FDC	1.45	92.8	0.34	0.45	DD5
3	6LRM	1.45	93.6	0.21	1.94	EQC
4	6IMI	1.46	94.4	0.28	2.62	AH6
5	6IMT	1.48	94.0	0.31	2.47	AK0
6	6IMD	1.50	94.1	0.23	1.99	AH9
7	7B9H	1.50	93.2	0.23	2.83	T3K
8	7CBJ	1.50	93.6	0.21	0.97	FTX
9	1XOQ	1.83	93.8	0.37	0.58	ROF
10	1OYN	2.00	90.9	0.43	0.63	ROL

Based on the ensemble docking process, in the virtual screening process, 25 test ligand compounds were docked to 20 structures at once, namely 10 PDE4B structures and 10 PDE4D structures with ten repetitions (**Table S1**). Ensemble docking is a computational drug discovery technique that accounts for protein flexibility by docking ligands to multiple conformations of a target protein, to identify more accurate binding predictions. Based on **Table 3**, The ligand with the highest binding affinity value indicated by the most negative value is compound 13 for inhibition of PDE4B and PDE4D, namely –10.90 ± 0.41 and –10.24 ± 0.39 kcal/mol. The lower Gibbs free energy (ΔG) indicates that the compound reacts more quickly and spontaneously. This

shows the potential and activity to interact and establish strong bonds with its target protein [47]. Compared with comparison compounds, such as rolipram, the binding energy values for PDE4B and PDE4D tend to be the same. At the same time, compound 13 has a greater affinity for PDEB than PDE4D, so it is predicted to have strong potential in selectively inhibiting the PDE4B enzyme.

Table 3 Binding energy (kcal/mol) of test ligands and comparison for PDE4B and PDE4D proteins.

Ligand	ΔG (kcal/mol) (Mean ± SD)		Ligand	ΔG (kcal/mol) (Mean ± SD)	
	PDE4B	PDE4D		PDE4B	PDE4D
13	–10.90 ± 0.41	–10.24 ± 0.39	8	–9.28 ± 1.24	–9.62 ± 0.36
12	–10.71 ± 1.07	–10.20 ± 0.41	5	–9.06 ± 1.10	–9.25 ± 0.36
11	–10.57 ± 1.00	–10.17 ± 0.31	7	–8.64 ± 1.68	–9.26 ± 0.51
15	–10.54 ± 0.94	–10.27 ± 0.36	6	–8.54 ± 1.82	–9.29 ± 0.61
9	–10.35 ± 0.65	–9.99 ± 0.34	25	–8.54 ± 1.75	–9.23 ± 0.46
10	–10.09 ± 1.38	–10.04 ± 0.33	22	–8.23 ± 1.73	–9.93 ± 0.55
24	–10.09 ± 0.98	–10.30 ± 0.48	19	–7.92 ± 2.16	–8.19 ± 0.66
14	–9.98 ± 0.82	–9.87 ± 0.48	17	–7.44 ± 2.87	–9.46 ± 0.56
23	–9.85 ± 0.81	–10.22 ± 0.62	18	–7.39 ± 3.14	–9.39 ± 0.32
1	–9.80 ± 1.39	–9.88 ± 0.65	21	–7.06 ± 2.24	–8.10 ± 0.29
4	–9.64 ± 1.09	–10.06 ± 0.60	20	–6.99 ± 2.73	–8.56 ± 0.80
2	–9.54 ± 0.76	–9.84 ± 0.52	CMP	–7.95 ± 0.55	–7.95 ± 0.67
16	–9.50 ± 1.43	–10.05 ± 0.34	ROF	–8.67 ± 0.51	–8.32 ± 0.29
3	–9.50 ± 0.88	–9.36 ± 0.55	ROL	–7.74 ± 0.53	–7.70 ± 0.63

All test compounds have a lower binding energy than the reference compound (rolipram), except for compounds 17, 18, 20 and 21. These results indicate that these compounds can potentially inhibit the PDE4B enzyme, including compounds 5, 13, 22 and 25, which will be further analyzed against MD and *in vitro*. Compounds 18 and 20 have lower affinity than the reference compounds and will be further analyzed to evaluate the relationship between the docking method, MD and *in vitro*. Moreover, compounds 5, 13, 18, 20, 22 and 25 have been isolated from *A. hunsteinii* and *A. cunninghamii* Indonesia, which can be used to analyse the relationship between data compounds that have low and high binding energy in the results of *in silico* and *in vitro*.

Cross-docking results were visualised using Ligplot$^+$ (2D) and Pymol 3.1.4 (3D) software to analyse interactions between ligands and receptors (**Figure S1**). Based on **Table 4**, the differences in the binding positions of atomic groups and bond distances in compound 13 to PDE4B and PDE4D affect the resulting binding energy. Compound 13 has three hydrogen bonds with a short bond distance to the PDE4B receptor, causing a low binding energy value. The key residues interacting with compound 13 are Asp124, Glu266, Lys354, Glu358, Asn132, His183, Leu152, Phe263, Leu242, Phe295, Met196, Asp241, Tyr382. The bonds involving polar residues such as Asp124 and Leu351 allow hydrogen interactions. The binding site location has more negatively charged residues interacting with the polar groups of compound 13. This suggests that PDE4B may be more affected by electrostatic interactions. The hydrophobic bond with the Asp241 residue is more stable, as evidenced by Al-Nema's study [5].

Table 4 Binding interactions of selected test compounds to PDE4B and PDE4D proteins.

Protein-Ligand complexes	Hydrogen bonds			Hydrophobic bonds
	Bond distance (Å)	Atoms on the ligand	Amino acid residues	
PDE4B				
Compound 5	2.85	C7"-OCH_3	His234	Asn395, Asp392, Asp275, Gln443, His, 278, Ile410, Leu393, Leu303, Met431, Met347, Phe414, Phe446, Ser282, Tyr403
	2.72	C5"-OH	Glu304	
	3.09	C4"=O	Asn283	
	2.94	C4'-OH	Thr407	
Compound 13	2.96	C5"-OH	Leu351	Asn132, Asp241, Gln266, Glu358, His83, His87, His127, Leu152, Leu242, Lys354, Met196, Phe263, Phe295, Phe355, Ser13, Tyr82
	2.40	C5-OH	Asp124	
	Mg-2.36	C5-OH		
Compound 18	3.26	C7"-OCH_3	Asn283	Cys432, His234, His278, Ile410, Ile450, Gln443, Glu413, Met431, Phe414, Phe44, Val281, Ser282, Ser429.
	2.86	C5"-OH	Gln417	
	3.12	C5-OH	Thr345	
	3.22		Met347	
Compound 20	3.08	C5"-OH	Glu304	Asn283, Asp346, Cys432, Gln284, Gln443, Gln417, Glu413, His234, His278, Ile450, Met431, Phe414, Phe446, Val281, Ser282, Ser429.
	3.06		Thr345	
	3.14		Mert347	
Compound 22	2.04-Mg-2.35	C4"=O	Asp128	Asn136, Gln137, Glu157, His87, Ile263, Leu246, Lys358, Met200, Phe267, Phe359, Phe299, Pro249, Tyr86.
	3.14	C5"-OH		
	2.82-Zn-2.01			
	2.82-Zn-2.05		His127	
	2.82-Zn-2.07		His91	
	2.82-Zn-2.13		Asp245	
	3.31	C4'-OH		
	3.32		Asn248	
Compound 25	3.11	C4"=O	Gln443	Asn283, His234, Ile410, Met347, Met431, Phe414, Phe446, Ser282, Ser442.
	2.67	C5-OH	Glu304	
	2.66-Mg-2.19	C4=O	Asp275	
CMP	2.98	C5-N	Asn395	Asp392, Gln443, Ile410, Met347, Phe414, Phe446
	3.12	N7	Asn395	
	2.95		Tyr233	
	3.08	P=O	His234	
	2.71-Zn-2.16		Asp392	
	2.71-Zn-2.16		His238	
	2.71-Zn-		His274	

Protein-Ligand complexes	Hydrogen bonds			Hydrophobic bonds
	Bond distance (Å)	Atoms on the ligand	Amino acid residues	
	2.71-Zn-		Asp275	
	2.35-Mg-2.11	P-O		
ROL	3.16	C1=O	Leu351	Gln292, His83, Ile259, Met196, Met352, Phe263, Phe295, Phe355, Tyr82.
ROF	3.30	C5-Cl	His87	Asn248, Gln296, Ile263, Met200, Met284, Phe267, Phe299, Phe359, Pro249, Ser295, Thr260, Trp259, Tyr256.
PDE4D				
Compound 5	2.85	C5"-OH	Gln210	Asn209, Asp201, His160, His204, Ile336, Met273, Met357, Phe340, Phe372, Pro356, Ser208.
	3.20	C4'-OH	Gln369	
Compound 13	3.00	C5"-OH	Gln343	Asn321, Asp272, Cys358, His160, Ile336, Met273, Val207, Phe340, Phe372, Thr271, Ser208.
	3.14			
	2.81	C4'"-OH	Glu230	
	3.31-Zn-2.01		Asp201	
	2.98	C4-OH	Gln369	
	2.93	C7-O-CH_3	Tyr159	
Compound 18	2.92	C5"-OH	Gln343	Asp272, Cys358, Glu339, His160, His204, Ile336, Ile376, Met357, Val207, Phe340, Phe372, Ser208.
	2.94	C5-OH	Met273	
	3.21		Thr271	
Compound 22	2.81	C7"-OH	His204	Asn209, Asp272, Glu230, His160, Ile336, Leu229, Leu319, Met273, Phe340, Ser208.
	2.90	C5-OH	Asp318	
	2.54-Mg-2.06		Asp201	
	3.12		Thr271	
Compound 20	3.03	C5"-OH	Glu230	Asn209, Asp272, Cys358, Glu339, His160, His204, Met357, Val207, Phe340, Phe372, Ser208, Ser355.
	2.95		Met273	
	3.25		Thr271	
	3.17	C5-OH	Gln343	
Compound 25	2.78-Mg-2.07	C4=O	Asp201	Asn209, Asp272, Gln210, Gly371, His160, Ile336, Ile376, Met357, Phe340, Phe372, Ser208, Tyr375.
	3.23	C5-OH	Met273	
	2.69		Glu230	
CMP	3.29	C6-N	Asn321	Ile336, Leu319, Met273,
	3.32	N1	Gln369	Phe372, Tyr159.
	3.12	O3'	His160	
	2.36-Mg-2.05	P=O	Asp201	
	2.45-Zn-2.05	P-O		

Protein-Ligand complexes	Hydrogen bonds			Hydrophobic bonds
	Bond distance (Å)	Atoms on the ligand	Amino acid residues	
	2.45-Zn-2.21		His200	
	2.45-Zn-2.13		Asp318	
	2.45-Zn-2.20		His164	
ROF	3.03	C16-Fe17	Thr499	Asn487, Gln535, His326, Ile502, Met439, Met523, Phe538, Tyr325.
ROL	3.14	C8-OCH_3	Gln369	Asp318, Asn321, His160, Ile336, Leu319, Met337, Met357, Phe340, Phe372, Ser368, Trp332, Tyr159, Thr333.
	2.86	O3		

In the case of PDE4D, the binding energy of compound 13 with the PDE4D receptor is higher, with six hydrogen bonds. The residues interacting with compound 13 are Asp201, Gln343, Gln369, Thr271, Met273, Phe340, Tyr159, Ile336, His160, Phe372, Ser208 and Asn321. In PDE4D, the interactions involve hydrogen bonds with polar residues (Asp201, Gln343) and hydrophobic interactions with aromatic residues (Phe340, Phe372). The differences in interactions of compound 13 with PDE4B and PDE4D may affect the binding affinity and have implications for the selectivity of the compound towards PDE4B or PDE4D.

Visualization of compound 13 interactions with PDE4B and PDE4D proteins can be seen in **Figure 2**. Hydrogen bonds are the most important specific interactions in the ligand-receptor interaction process. Hydrogen bond interactions regulate the stability of the complexes formed [48]. Compound 13 has a hydrogen bond with the Mg metal ion in the PDE4B protein, whereas, in PDE4D, it does not interact with the Mg metal ion but with the Zn metal ion. Gangwal *et al*. [11] reported that most selective PDE4B inhibitors showed charge interactions with magnesium metal ions. Residue Asp124 controls inhibitor access to magnesium metal ions. Meanwhile, in PDE4D inhibitor. the selective inhibitor cannot form charge interactions with magnesium ions. Competitive inhibition of the PDE4B enzyme by mimicking the substrate and binding to the enzyme's active site so that the enzyme experiences reduced or no activity. Hydrogen bond acceptors were identified as mainly responsible for the inhibition of PDE4B. In contrast, hydrogen bond acceptors and hydrophobic groups were found to be responsible for the inhibition of PDE4D [10].

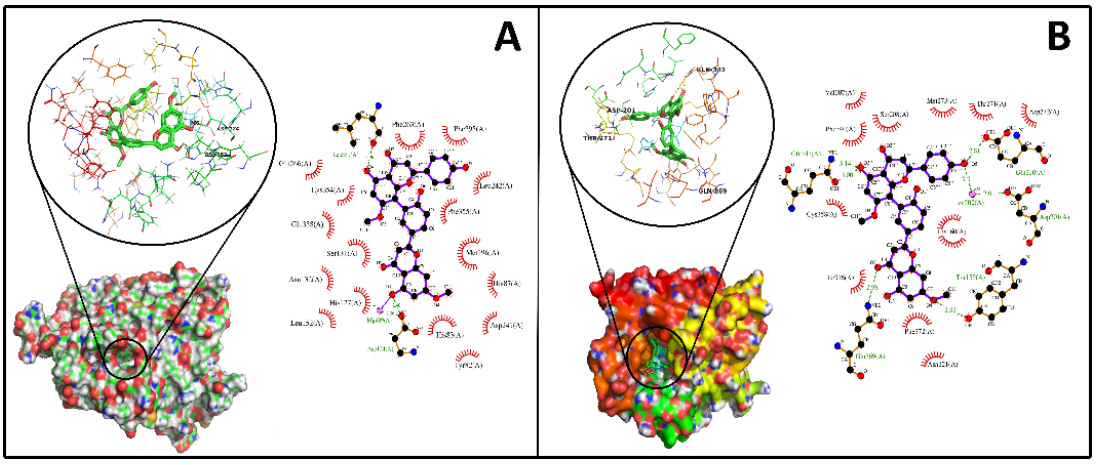

Figure 2 2D and 3D visualization of the interaction between compound 13 on (A) PDE4B and PDE4D (B).

Stability and potency of biflavonoid ligands as PDE4B and PDE4D inhibitors

The MM/GBSA method is an implicit solvation method for evaluating the binding free energy of ligands to biological macromolecules (proteins), usually based on molecular dynamics simulations [49]. The binding energy values of each complex were then averaged to obtain the MM/GBSA binding energy values listed in **Table 5**. The PDE4B-compound 13 complex had the lowest average binding energy value of –49.56 ± 4.12 kcal/mol. The PDE4D-compound 5 complex had the lowest binding energy value of –45.09 ± 4.11 kcal/mol. Based on **Figure 3**, compound 13 exhibits the best and most stable binding to PDE4B among the other compounds. Meanwhile, the PDE4D-13 complex has fluctuating binding. Compound 5 showed the best binding to PDE4D compared to other compounds. Stable protein-ligand interactions during MD simulations support our previous docking results and confirm the role of the new molecule as a potent PDE4B inhibitor.

Table 5 Average MM/GBSA binding energy of selected test ligands and comparison ligands with PDE4B and PDE4D proteins for 100 ns.

Ligand	Binding energy (MM/GBSA) (kcal/mol) (Mean ± SD)	
	PDE4B	PDE4D
7,7″-di-*O*- methylamentoflavone (**13**)	–49.56 ± 4.12	–39.77 ± 5.21
7,4′,4‴-tri-*O*-methylrobustaflavone (**25**)	–43.05 ± 6.48	–30.20 ± 4.16
7,4′,7″,4‴-tetra-*O*-methylcupressuflavone (**20**)	–39.66 ± 5.60	–33.33 ± 5.78
7,4‴-di-*O*-methylcupressuflavone (**22**)	–33.45 ± 7.28	–34.02 ± 5.73
7,4′,7″-tri-*O*-methylcupressuflavone (**18**)	–27.37 ± 9.53	–31.41 ± 4.38
7,4‴,7″-tri-*O*-methylagathisflavone (**5**)	–24.23 ± 4.93	–45.09 ± 4.11
ROL	–28.28 ± 2.95	–23.31 ± 3.32
CMP	–25.19 ± 6.74	–1.79 ± 6.23
ROF	–19.63 ± 4.44	–24.70 ± 5.67

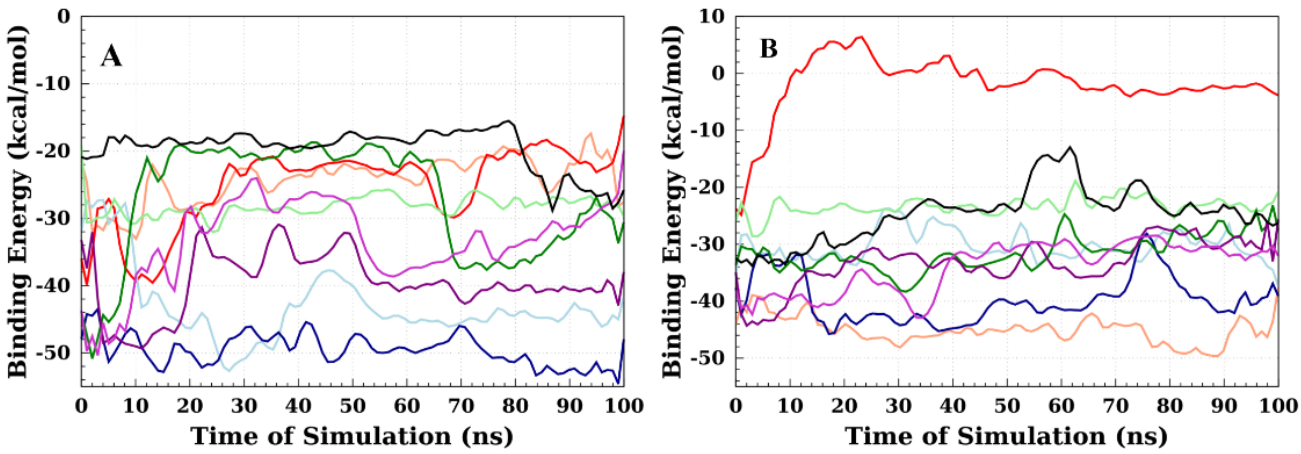

Figure 3 Stability of MM/GBSA binding energy of selected test compounds on (A) PDE4B and (B) PDE4D during a simulation time of 100 ns (orange = compound 5; dark blue = compound 13; green = compound 18; purple = compound 20; pink = compound 22; light blue = compound 25; red = CMP; light green = ROL; black = ROF).

The RMSD values of protein-ligand complexes are represented on a graph of RMSD values over a simulation time of 100 ns, as shown in **Figure 4**. RMSD is the average atomic displacement during the simulation relative to a reference structure, usually the first frame of the simulation or a crystallographic structure. RMSD is useful for analysing time-dependent structural motion. It is often used to distinguish whether a structure is stable in the simulation time scale or deviates from the initial coordinates [40]. In **Figure 4(A)**, most structures show an initial increase in RMSD (up to 20 ns) before stabilizing their fluctuations. Meanwhile, in **Figure 4(B)**, the RMSD value of PDE4D in compound **13** shows a significant increase of approximately 3.0 Å after 40 ns, in contrast to the RMSD in compound PDE4B-**13**, which remains more stable. This value indicates that the complex undergoes a significant change or shift in position as the simulation progresses. A high RMSD value indicates a change in structural conformation during the simulation, which indicates unstable structural quality.

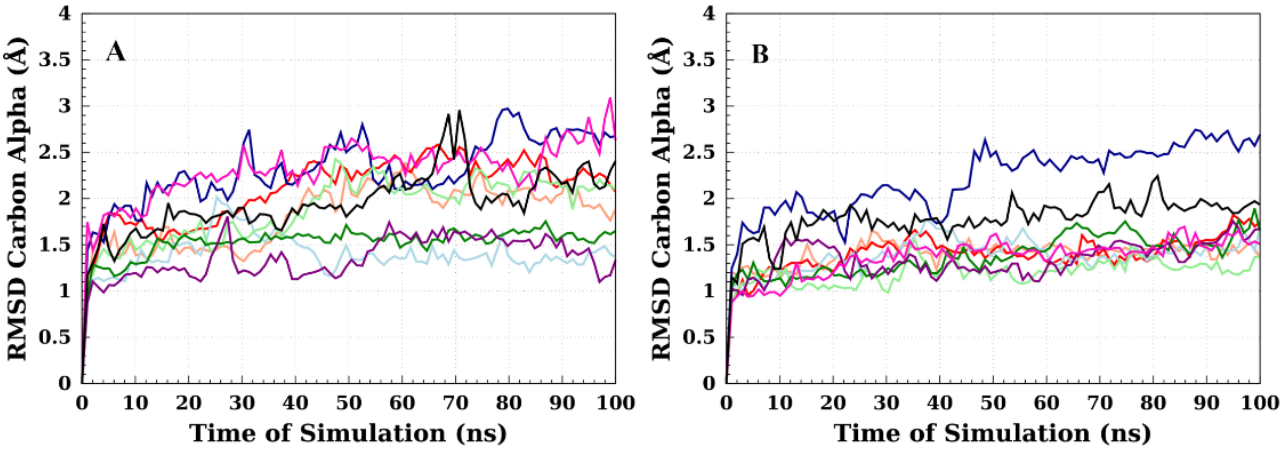

Figure 4 RMSD of selected protein-ligand complexes (A) PDE4B and (B) PDE4D during 100 ns of simulation run (orange = compound 5; dark blue = compound 13; green = compound 18; purple = compound 20; pink = compound 22; light blue = compound 25; red = CMP; light green = ROL; black = ROF).

Hydrogen bond analysis is carried out by observing the donor-acceptor pair between the target protein and the selected ligand and the fraction of hydrogen bonds formed. The primary marker of specificity and molecular interaction between protein complexes and inhibitors is the formation of hydrogen bonds [39]. The hydrogen bonds formed for PDE4 subtype proteins with each compound studied were observed for all trajectories using 100 ns MD simulation trajectories presented in **Table 6**. They were ranked among all the hydrogen bonds formed in each protein-ligand complex. The five highest ties taken during the simulation are based on the most considerable fraction value. The fraction shows the proportion or probability of the hydrogen bond interaction in the simulation or analysis. Higher fraction values indicate more frequent binding. Compound 13 with PDE4B forms hydrogen bonds with residues Leu349, Gln264, Gln290, Ser289 and Glu356. Hydrogen bonds with residue Leu349 have a higher fraction (0.49) and an average bond distance of 2.77 Å, indicating strong and frequent interactions. The interactions are more dominant involving the carbonyl group (C4"=O) and hydroxyl groups (C4'-OH and C5-OH) of compound 13. Compound 13 forms of hydrogen bonds with residues Gln265, Ser130, Met195 and Ser290. In PDE4D, the interaction with Gln265 has the highest fraction (0.36), with a bond distance of 2.72 Å. However, interactions with other residues have lower fractions and slightly longer distances, indicating a possible lower stability compared to PDE4B.

Table 6 Hydrogen bonds in selected protein-ligand complexes during 100 ns simulation.

Complex	Acceptor	Donor	Fraction	Mean bond distance (Å)
PDE4B				
Compound 5	Gln289	Compound 5 (C4'-OH)	0.11	2.71
	Compound 5 (C4'-OH)	Tyr249	0.09	2.86
	Tyr249	Compound 5 (C4'-OH)	0.04	2.84
	Asp192	Compound 5 (C5"- OH)	0.01	2.71
	Compound 5 (C4"=O)	Gln130	0.01	2.88
Compound 13	Leu349	Compound 13 (C4'-OH)	0.49	2.77
	Compound 13 (C4=O)	Gln264	0.26	2.88
	Compound 13 (C4"=O)	Gln290	0.11	2.88
	Compound 13 (C4"=O)	Ser289	0.03	2.76
	Glu356	Compound 13 (C5-OH)	0.03	2.69
Compound 18	Met186	Compound 18 (C4'"-OH)	0.19	2.74
	Compound 18 (C7-OCH_3)	Gln256	0.06	2.91
	Compound 18 (C4=O)	Hie117	0.05	2.9
	Compound 18 (C5-OH)	Hie117	0.04	2.91
	Hie189	Compound 18 (C4'"-OH)	0.04	2.86
Compound 20	Compound 20 (C5"-OH)	Gln256	0.15	2.9
	Compound 20 (C7"-OCH_3)	Hie73	0.03	2.9
	Compound 20 (C7-OCH_3)	Gln256	0.01	2.93
	Compound 20 (C4'"-OH)	Ser187	0.002	2.84
	Compound 20 (C4"=O)	Ser268	0.001	2.75
Compound 22	Asp243	Compound 22 (C4'-OH)	0.74	2.7
	Hie85	Compound 22 (C5"-OH)	0.13	2.83
	Asp243	Compound 22 (C4'-OH)	0.13	2.74
	Compound 22 (C4"=O)	Met198	0.12	2.9
	Tyr84	Compound 22 (C7"-OH)	0.07	2.74
Compound 25	Asp196	Compound 25 (C5-OH)	0.79	2.64
	Ser198	Compound 25 (C5-OH)	0.07	2.79
	Asp196	Compound 25 (C5-OH)	0.05	2.65
	Compound 25 (C4=O)	Asn133	0.01	2.91
	Compound 25 (C7-OCH_3)	Gln134	0.01	2.88
CMP	CMP (N1)	Gln289	0.15	2.9
	Gln289	CMP (C6-NH)	0.14	2.87
	CMP (O3')	Hip80	0.02	2.85
	CMP (P=O)	Hip80	0.01	2.88
	Gln289	CMP (C6-NH)	0.01	2.88
ROL	Tyr80	ROL (NH)	0.11	2.89

Complex	Acceptor	Donor	Fraction	Mean bond distance (Å)
	ROL (C1=O)	Tyr80	0.01	2.75
	Ile257	ROL (NH)	0.005	2.88
	ROL (C8-OCH_3)	Ser289	0.002	2.84
	ROL (C8-OCH_3)	Gln290	0.001	2.89
ROF	ROF (F18)	Gln294	0.11	2.89
	ROF (F17)	Gln294	0.01	2.88
	ROF (F17)	Gln294	0.003	2.9
	ROF (O19)	Gln294	0.002	2.93
	ROF (F18)	Gln294	0.001	2.86
PDE4D				
Compound 5	Thr248	Compound 5 (C4'-OH)	0.68	2.81
	Asn236	Compound 5 (C4'-OH)	0.08	2.76
	Compound 5 (C4'''-OCH_3)	Gln258	0.05	2.88
	Compound 5 (C4'-OH)	Gln284	0.01	2.92
	Compound 5 (C4'''-OCH_3)	Hie75	0.01	2.89
Compound 13	Gln265	Compound 13 (C4'''-OH)	0.36	2.72
	Compound 13 (C4'''-OH)	Ser130	0.14	2.84
	Compound 13 (C4'''-OH)	Gln265	0.05	2.9
	Met195	Compound 13 (C4'-OH)	0.05	2.8
	Compound 13 (C4=O)	Ser290	0.02	2.75
Compound 18	Compound 18 (C4=O)	Gln283	0.05	2.86
	Met187	Compound 18 (C4'''-OH)	0.03	2.76
	Ser269	Compound 18 (C5''- OH)	0.02	2.76
	Compound 18 (C4'-OCH_3)	Gln283	0.01	2.88
	Compound 18 (C7''-OCH_3)	Hie74	0.01	2.91
Compound 20	Asp114	Compound 18 (C5-OH)	0.84	2.63
	Compound 20 (C7''-OCH_3)	Hie73	0.32	2.87
	Thr184	Compound 18 (C5-OH)	0.06	2.74
	Compound 20 (C7-OCH_3)	Hie117	0.04	2.91
	Asp114	Compound 18 (C5-OH)	0.01	2.89
Compound 22	Asp115	Compound 22 (C5-OH)	0.99	2.6
	Gly120	Compound 22 (C7''-OH)	0.76	2.72
	Compound 22 (C7''-OH)	Hie118	0.17	2.92
	Compound 22 (O1)	Hie74	0.09	2.92
	Val121	Compound 22 (C7''-OH)	0.05	2.73
Compound 25	Gly292	Compound 25 (C7''-OH)	0.16	2.73
	Compound 25 (C4'''-OCH_3)	Ser285	0.07	2.89
	Compound 25 (C4=O)	Gln131	0.02	2.88

Complex	Acceptor	Donor	Fraction	Mean bond distance (Å)
	Asp193	Compound 25 (C5-OH)	0.02	2.69
	Compound 25 (C4"=O)	Met278	0.01	2.89
CMP	Gln282	CMP (C6-NH)	0.48	2.73
	CMP (O3')	Hie73	0.14	2.89
	Asn234	CMP (C6-NH)	0.09	2.75
	Asn234	CMP (C6-NH)	0.07	2.77
	Gln282	CMP (C6-NH)	0.02	2.73
ROL	ROL (C1=O)	Hie75	0.06	2.85
	ROL (C8-OCH_3)	Gln284	0.06	2.89
	ROL (C1=O)	Ser283	0.68	2.81
	ROL (C1=O)	Asn277	0.08	2.76
	Gly286	ROL (NH)	0.05	2.88
ROF	ROF (O15)	Gln287	0.01	2.92
	Tyr77	ROF (N7-H)	0.01	2.89
	ROF (O19)	Gln287	0.36	2.72
	Ser286	ROF (N7-H)	0.14	2.84
	ROF (N3)	Hie78	0.05	2.9

Enzymatic Inhibition of PDE4B and PDE4D

Cytotoxic activities of biflavonoids were evaluated against MCF-7 (human breast cancer cell line) using MTT assay as in the previous report (**Table 7** and **Figure S2**). By [37], Among the isolated biflavonoids from the leaves of *A. cunninghami*, the 7,7″-di-O-methylamentoflavone (13) shows the highest *in vitro* activity estimate (IC_{50} = 150.04 ± 23.97 µM) followed by the7,4′,7″,4‴-tetra-*O*-methylcupressuflavone (20) (IC_{50} =1,301.80 ± 173.86 µM) and 7,4',4"'-tri-*O*-methylrobustaflavone (25) (IC_{50} = 2503.91 ± 206.25 µM). By [19] and [24], biflavonoid compounds isolated from *A. hunsteinii* K. Schum leaves have IC_{50} values against MCF-7 cells of 22 < 18 < 5 respectively. The biflavonoids from *A. cunninghamii* and *A. hunsteinii* that were most active in inhibiting MCF-7 cells were 13 and 22. Compound 13 was identified as a potent cytotoxic compound in A549 cells, however, the selectivity index was the lowest because 13 showed cytotoxicity in the normal human lung fibroblast MRC-5 cell line [50]. Amentoflavone was not cytotoxic to Human Peripheral Lymphocytes (normal cell lines) in the trypan blue exclusion assay. The cell viability of MCF-7 was inversely proportional to the treatment dose (amentoflavone) as the cell inhibition increased when the concentration increased from 6.25 - 100 µg/ml. The results revealed that the amentoflavone is highly efficient against MCF-7 cells [51]. Cupressoflavone showed high cytotoxic selectivity for prostate cancer cells (PC-3) with an IC_{50} value of 19.9 µM while showing no cytotoxicity against the normal prostate cell line (PNT2) [52]. Biflavonoids strongly affect cancer cells with little effect on normal cell proliferation, suggesting a therapeutic potential against cancer [53]. PDE4 has been identified in MCF-7 human breast cancer cells and is known to contribute to the degradation of intracellular cAMP, leading to reduced cAMP levels. PDE4 inhibition may contribute directly to antiproliferative effects via cAMP elevation and thus, cytotoxicity observed in PDE4-targeting compounds [54].

Table 7 IC_{50} values of biflavonoids against inhibition of PDE4B and PDE4D enzymes and the cytotoxic effects of biflavonoids on MCF-7 cell.

Compounds	Inhibitory activity IC_{50} (μM) (Mean ± SD)		MCF-7 Cytotoxicity IC_{50} (μM)
	PDE4B	PDE4D	
7,7″-di-*O*-methylamentoflavone (13)	13.9 ± 2.38	15.02 ± 3.5	150.04 ± 23.97 [37]
7,4‴-di-*O*-methylcupressuflavone (22)	121.7 ± 7.3	130 ± 2.7	11.54 ± 3.4 [24]
7,4',4"'-tri-*O*-methylrobustaflavone (25)	225.10 ± 6.3	218.55 ± 1.35	2,503.91 ± 206.25 [37]
7,4′,7″-tri-*O*-methylcupressuflavone (18)	451.45 ± 6.35	494.8 ± 65.8	91.74 ± 5.6 [19]
7,4‴,7″-tri-*O*-methylagathisflavone (5)	830.15 ± 13.15	846.6 ± 14.7	314.44 ± 25.0[19]
7,4′,7″,4‴-tetra-*O*-methylcupressuflavone (20)	1,357 ± 1	1,279 ± 68	1,301.8 ± 173.86 [37]
Rolipram [55]	0.13	0.24	-
Roflumilast [6]	8.4×10^{-4}	6.8×10^{-4}	-

The *in vitro* anti-inflammatory activity of compounds 5, 18 and 22 obtained from the leaves of *A. hunsteinii* K. Schum and compounds 13, 20 and 25 obtained from the leaves of *A. cunninghamii* were evaluated through inhibition of the PDE4B and PDE4D enzymes using ELISA. The inhibitory activity used as a parameter is the IC_{50} value. The IC_{50} value represents the concentration of a compound that inhibits 50% of the activity against proteins (**Table S2**). The smaller the IC_{50} value indicates the greater the inhibitory activity of the PDE4B and PDE4D enzymes. Based on **Table 7**, compound 13 shows the best activity with an IC_{50} value of 13.9 ± 2.38 μM against PDE4B inhibition and 15.02 ± 3.5 μM against PDE4D and can be categorized as very strong. This indicates that compound 13 is more potent of inhibiting the PDE4B enzyme than PDE4D. Compound 22 has an IC_{50} value between 100 - 150 μM, categorized as medium. Meanwhile, compounds 5, 18, 20 and 25 showed IC_{50} values > 200 μM, which were categorized as very weak according to [56]. The IC_{50} value of compound 13 is higher than that of conventional drugs such as PDE4 inhibitors such as rolipram and roflumilast. Compound 13 is a selective and potent inhibition of the PDE4 isoform (IC_{50} =1.48 ± 0.21 mM) from PDE1, PDE2, PDE3 and PDE5 isoform and was almost as active as the reference drug rolipram (IC_{50} = 1.1 ± 0.2 mM) [9]. The experimental IC_{50} values of compound 13 above were similar to the virtual screening affinity binding values (**Tables 3 - 5**). This contributed to confirming the agreement of results between experimental and virtual screening.

Statistical correlation between PDE4B/PDE4D inhibition and cytotoxicity

To investigate the association between cytotoxicity and PDE4B/PDE4D inhibition, we used simple linear regression analysis (**Figure 5**) with data from **Table 7**. The coefficient of determination (R^2) used in this investigation is based on [57]. The correlation coefficient (R^2) between PDE4B inhibition and MCF-7 cytotoxicity is 0.0317 (*p-value* > 0.05). Furthermore, the correlation coefficient (R^2) between PDE4D inhibition and MCF-7 cytotoxicity is 0.0215 (*p-value* > 0.05). These findings suggest that there is no statistically significant relationship between PDE4B/PDE4D inhibition and cytotoxicity in MCF-7 cells. Thus, the observed suppression of PDE4B and PDE4D appears to be a pharmacological action rather than a result of general cytotoxicity or cell death.

Some compounds showed non-synergistic patterns, such as modest cytotoxicity but significant PDE4 inhibition (compound 22), or vice versa. We believe this could be due to a variety of variables, including changes in intracellular chemical accumulation, microenvironmental pH, solubility, or differential engagement with off-target proteins. Notably, several biflavonoids inhibited PDE4 at concentrations far below their cytotoxic IC_{50}, indicating the presence of a therapeutic agent [54]. Compound 13 suppressed PDE4B at 13.9 μM but exhibited cytotoxicity at 150.04 μM. Compound 22 exhibited increased cytotoxicity (IC50 = 11.54 μM), suggesting overlapping pathways or reduced safety margins.

These findings are consistent with prior research on biflavonoids such as amentoflavone and cupressuflavone, which were found to have strong enzymatic inhibition and anti-inflammatory activity in non-cancer cell lines [52,53]. Furthermore, inhibition of PDE4 has been demonstrated to have no inherent deleterious effects in epithelial or non-immune models [5]. These findings suggest that, while some biflavonoids may have cytotoxic effects, their PDE4 inhibitory activity is mechanistically different. Future investigations with immune-relevant or normal cell lines are required to validate selectivity and eliminate any off-target damage.

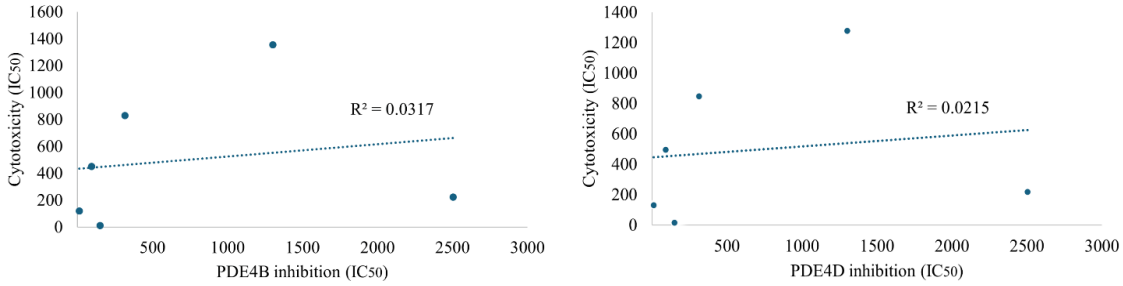

Figure 5 Simple linear regression for the correlation between (A) PDE4B and (B) PDE4D inhibition and cytotoxicity.

The relationship between structure and biological activity of biflavonoids

The relationship between the structure and activity of biflavonoids is not only influenced by the amount, but also the position of the methoxy, hydroxyl and basic framework groups in the biflavonoid structure plays an important role in the relationship with the inhibitory activity of PDE4B and PDE4D (**Figure 6**). Compound 13 exhibited the best activity, with IC_{50} values of 13.9 ± 2.38 μM for PDE4B inhibition and 15.02 ± 3.5 μM for PDE4D. Compound 13 is known to have two hydroxyl groups at C4′ and C4‴, where the hydroxyl group at C4′ binds directly to the PDE4D protein. Compound 22 exhibits quite good activity (IC_{50} < 150 μM) in inhibiting PDE4B through hydrogen bonding to the C4′ hydroxyl group and PDE4D is directly bonded to C7″, as predicted by *in silico* analysis. Compounds 13 and 22 have similarities in that they have two hydroxyl groups with one C4′ position in ordinary, but the amentoflavone group compound (13), which has a C3′-C8″ linkage, has better inhibitory activity than the cupressuflavone group (22), which has a C8-C8″ linkage. The substituent at the 4′ position of one benzene ring significantly affects on the PDE4 inhibitory activity [58]. 4'-OH is important for activity because the presence of 4'-OH has maintained its inhibitory activity [59]. In the cupresuflavone derivative group, the IC_{50} value of compound 22 < 18 < 20 was obtained, followed by a decrease in the hydroxyl group; this indicates that the greater the presence of hydroxyl groups in the cupresuflavone group, the greater the inhibition of the PDE4B and PDE4D enzymes. Substitution by the methoxy group at C-7", as occurs in compounds 5, 18 and 20, causes a decrease in inhibitory activity on both enzymes; on the other hand, strong inhibitory activity is obtained from the amentoflavone group, namely compound 13.

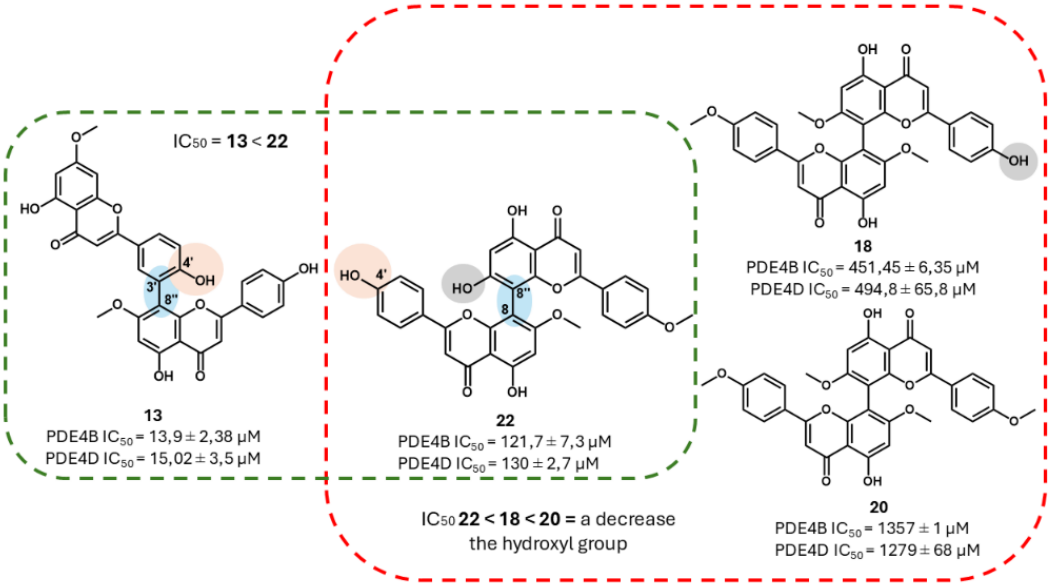

Figure 6 Summarization of structure-activity relationship (SAR) analysis.

Compound **13** displays strong alignment between computational and experimental data. Additionally, the predicted inhibition constant (Ki value) in the molecular docking analysis. The smaller the value of Ki the lower will be the probability of dissociation and hence higher will be the inhibiton. It is calculated as Ki = exp(deltaG/(R*T)) where deltaG is the free energy of binding, R is the gas constant (1.987 cal K^{-1} mol^{-1}) and T is the temperature (312 K). The results of the calculation of the inhibition constant (Ki) show that compound 13 gives a Ki value of 19.9 nM against PDE4B and 68.2 nM against PDE4D. This further confirms that the binding of compound 13 is stronger against PDE4B than PDE4D. Unfortunetly, several other compounds (e.g., 20, 25) exhibit good predicted affinities (**Table 5**) but low experimental activity (**Table 7**). This may be due to limitations in docking such as docking flexibility, solvation effects that affect the results. Autodock Vina overlooks the presence of water molecules in its screening process, which may lead to an underestimation of the interaction between ligands and water. It is known that water molecules play an important role in protein-ligand binding; however, due to the difficulty of explicitly determining the exact position of water molecules around the protein, most of the existing docking and scoring functions use a coarse-grained approach for speed and efficiency reasons. Second, another important issue is the rigidity of the protein structure in the docking protocol, which can play a major role in predicting the properties of the discovered compounds [60]. This docking does not consider the flexibility of the protein. Thus, experimental data is essential to obtain accurate results.

Despite promising findings, this study has limitations. The absence of *in vivo* validation restricts the direct applicability of our findings to physiological conditions. Additionally, the correlation between PDE4 inhibition and systemic inflammatory response remains to be fully explored. To address these limitations, future studies will involve animal models to assess the pharmacokinetics, toxicity and overall efficacy of the identified biflavonoids. Biomarker analysis, including TNF-α, IL-6 and COX-2 inhibition, will be conducted to strengthen the anti-inflammatory claim of these compounds. Previous studies have demonstrated that *in silico* and *in vitro* approaches provide a reliable foundation for early-stage drug discovery [2,41,49,61], supporting the rationale for our methodological framework. Moreover, while the *in vitro* results provide strong preliminary evidence, the lack of *in vivo* validation limits the direct translational relevance of this study, necessitating further preclinical assessments.

Conclusions

This study highlights the significant anti-inflammatory potential of biflavonoid compounds derived from the genus *Araucaria*. *In silico* and *in vitro* analyses, 7,7″-di-*O*-methylamentoflavone emerged as a

promising selective PDE4B inhibitor, demonstrating potent inhibitory activity and high binding affinity. These findings underline its potential as a lead compound for anti-inflammatory drug development. While this research offers valuable insights into biflavonoid interactions with PDE4 enzymes, further investigations, particularly *in vivo* studies, are essential to validate their therapeutic potential. These future efforts will contribute to the advancement of biflavonoid-based anti-inflammatory drugs with improved efficacy and safety profiles.

Acknowledgements

This research was supported by the Directorate General of Higher Education, Research and Technology, Ministry of Education, Culture, Research and Technology of Indonesia, through the Master's to Doctoral Education Program for Superior Undergraduates (PMDSU), by the 2024 and 2025 research program implementation contract number: 027/E5/PG.02.00.PL/2024 and 006/C3/DT.05.00/PL/2025, which provided financial support for this study. The authors would also like to acknowledge the computational facilities provided by the High-Performance Computing Laboratory, IPB University and the *in vitro* assay facilities provided by the Primate Research Center, IPB University, Indonesia.

Declaration of Generative AI in Scientific Writing

The only applications of generative AI were in language editing and clarity enhancement. It did not contribute to the conclusions, data analysis, or scientific substance. The authors retain all scientific accountability.

CRediT Author Statement

Nafisah: Conceptualisation, Investigation, Data curation, Writing – original draft. **Budi Arifin:** Methodology, Validation, Supervision, Writing – review & editing. **Setyanto Tri Wahyudi:** Molecular dynamics simulation, Software, Formal analysis. **Uus Saepuloh:** *In vitro* assay, Resources, Validation. **Kurniawanti:** Investigation, Data curation. **Silmi Mariya:** In vitro experiment, Data acquisition. **Purwantiningsih Sugita:** Conceptualisation, Supervision, Funding acquisition, Writing – review & editing.

References

[1] SI Grivennikov, FR Greten and M Karin. Immunity, Inflammation and Cancer. *Cell* 2010; **140(6)**, 883-899.

[2] K Komatsu, JY Lee, M Miyata, JH Lim, H Jono, T Koga, H Xu, C Yan, H Kai and JD Li. Inhibition of PDE4B suppresses inflammation by increasing expression of the deubiquitinase CYLD. *Nature Communications* 2013; **4**, 1684.

[3] T Peng, J Gong, Y Jin, Y Zhou, R Tong, X Wei, L Bai and J Shi. Inhibitors of phosphodiesterase as cancer therapeutics. *European Journal of Medicinal Chemistry* 2018; **150**, 742-756.

[4] L Crocetti, G Floresta, A Cilibrizzi and MP Giovannoni. An overview of PDE4 inhibitors in clinical trials: 2010 to early 2022. *Molecules* 2022; **27(15)**, 4964.

[5] M Al-Nema, A Gaurav and VS Lee. Docking based screening and molecular dynamics simulations to identify potential selective PDE4B inhibitor. *Heliyon* 2020; **6(9)**, e04856.

[6] J Jin, F Mazzacuva, L Crocetti, MP Giovannoni and A Cilibrizzi. PDE4 inhibitors: Profiling hits through the multitude of structural classes. *International Journal of Molecular Sciences*; **24(14)**, 11518.

[7] H Li, J Zuo and W Tang. Phosphodiesterase-4 inhibitors for the treatment of inflammatory diseases. *Frontiers in Pharmacology* 2018; **9**, 1048.

[8] JE Phillips. Inhaled phosphodiesterase 4 (PDE4) inhibitors for inflammatory respiratory diseases. *Frontiers in Pharmacology* 2020; **11**, 259.

[9] M Chaabi, C Antheaume, B Weniger, H Justiniano, C Lugnier and A Lobstein. Biflavones of decussocarpus rospigliosii as phosphodiesterases inhibitors. *Planta Medica* 2007; **73(12)**, 1284-1286.

[10] A Gaurav and V Gautam. Pharmacophore based virtual screening approach to identify selective PDE4B inhibitors. *Iranian Journal of Pharmaceutical Research* 2017; **16(3)**, 910-923.

[11] RP Gangwal, MV Damre, NR Das, GV Dhoke, A Bhadauriya, RA Varikoti, SS Sharma and AT Sangamwar. Structure based virtual screening to identify selective phosphodiesterase 4B inhibitors. *Journal of Molecular Graphics and Modelling*

2015; **57**, 89-98.

[12] M Rahman, M Riaz and UR Desai. Synthesis of biologically relevant biflavanoids - a review. *Chemistry and Biodiversity* 2007; **4(11)**, 2495-2527.

[13] B Gil, MJ Sanz, MC Terencio, R Gunasegaran, M Payá and MJ Alcaraz. Morelloflavone, a novel biflavonoid inhibitor of human secretory phospholipase A2 with anti-inflammatory activity. *Biochemical Pharmacology* 1997; **53(5)**, 733-740.

[14] T Banerjee, G Valacchi, VA Ziboh and A Vliet. Inhibition of TNFα-induced cyclooxygenase-2 expression by amentoflavone through suppression of NF-κB activation in A549 cells. *Molecular and Cellular Biochemistry* 2002; **238(1-2)**, 105-110.

[15] JK Son, MJ Son, E Lee, TC Moon, KH Son, CH Kim, HP Kim, SS Kang and HW Chang. Ginkgetin, a biflavone from Ginko biloba leaves, inhibits cyclooxygenases-2 and 5-lipoxygenase in mouse bone marrow-derived mast cells. *Biological and Pharmaceutical Bulletin* 2005; **28(12)**, 2181-2184.

[16] X Su, ZH Zhu, L Zhang, Q Wang, MM Xu, C Lu, Y Zhu, J Zeng, JA Duan and M Zhao. Anti-inflammatory property and functional substances of *Lonicerae japonicae* Caulis. *Journal of Ethnopharmacology* 2021; **267**, 113502.

[17] HP Kim, H Park, KH Son, HW Chang and SS Kang. Biochemical pharmacology of biflavonoids: Implications for anti-inflammatory action. *Archives of Pharmacal Research* 2008; **31(3)**, 265-273.

[18] YM Lin, MT Flavin, R Schure, FC Chen, R Sidwell, DL Barnard, JH Huffman and ER Kern. Antiviral activities of biflavonoids. *Planta Medica* 1999; **65(2)**, 120-125.

[19] DD Agusta, H Dianhar, DUC Rahayu, IH Suparto and P Sugita. Anticancer and antivirus activities of two biflavonoids from Indonesian *Araucaria hunsteinii* K Schum Leaves. *Journal of Human University (Natural Science)* 2022; **49(3)**, 169-177.

[20] MK Lee, SW Lim, H Yang, SH Sung, HS Lee, MJ Park and YC Kim. Osteoblast differentiation stimulating activity of biflavonoids from *Cephalotaxus koreana*. *Bioorganic & Medicinal Chemistry Letters* 2006; **16(11)**, 2850-2854.

[21] O Kunert, RC Swamy, M Kaiser, A Presser, S Buzzi, AVNA Rao and W Schühly. Antiplasmodial and leishmanicidal activity of biflavonoids from Indian *Selaginella bryopteris*. *Phytochemistry Letters* 2008; **1(4)**, 171-174.

[22] T Okoko. *In vitro* antioxidant and free radical scavenging activities of *Garcinia kola* seeds. *Food and Chemical Toxicology* 2009; **47(10)**, 2620-2623.

[23] JH Hwang, H Choi, ER Woo and DG Lee. Antibacterial effect of amentoflavone and its synergistic effect with antibiotics. *Journal of Microbiology and Biotechnology* 2013, **23(7)**, 953-958.

[24] P Sugita, DD Agusta, H Dianhar, IH Suparto, Kurniawanti, DUC Rahayu and L Irfana. The cytotoxicity and SAR analysis of biflavonoids isolated from *Araucaria hunsteinii* K. Schum. leaves against MCF-7 and HeLa cancer cells. *Journal of Applied Pharmaceutical Science* 2023; **13(10)**, 199-209.

[25] CS Estevam, FM Oliveira, LM Conserva, LDFCO Lima, ECP Barros, ACP Barros, EMM Rocha and E Andrade. Constituintes químicos e avaliação preliminar *in vivo* da atividade antimalárica de *Ouratea nitida* Aubl (Ochnaceae). *Revista Brasileira de Farmacognosia* 2005; **15(3)**, 195-198.

[26] Nafisah, P Sugita, B Arifin and ST Wahyudi. Biflavonoid anti-inflammatory activity of the araucariaceae family—a review. *Tropical Journal of Phytochemistry and Pharmaceutical Sciences* 2024; **3(9)**, 411-423.

[27] N Ilyas, M Ilyas, W Rahman, M Okigawa and N Kawano. Biflavones from the leaves of *Araucaria excelsa*. *Phytochemistry* 1978; **17(5)**, 987-990.

[28] N Parveen, HM Taufeeq and NU Khan. Biflavones from the leaves of *Araucaria araucana*. *Journal of Natural Products* 1987; **50(2)**, 332-333.

[29] AM Freitas, MTR Almeida, CR Andrighetti-Fröhner, FTGS Cardozo, CRM Barardi, MR Farias and CMO Simões. Antiviral activity-guided fractionation from *Araucaria angustifolia* leaves extract. *Journal of Ethnopharmacology* 2009; **126(3)**, 512-517.

[30] J Chen, ML Yang, J Zeng and K Gao. Antimicrobial activity of *Araucaria cunninghamii*

sweet and the chemical constituents of its twigs and leaves. *Phytochemistry Letters* 2013; **6(1)**, 41-45.

[31] C Frezza, DD Vita, L Fonti, O Giampaoli, CD Bosco, F Sciubba, A Venditti, C Scintu and F Attorre. Secondary metabolites of *Araucaria cunninghamii* Mudie from central Italy. *Plant Biosystems - An International Journal Dealing with All Aspects of Plant Biology* 2024; **158(4)**, 589-594.

[32] AN Talaat, SS Ebada, RM Labib, A Esmat, FS Youssef and ANB Singab. Verification of the anti-inflammatory activity of the polyphenolic-rich fraction of Araucaria bidwillii Hook. using phytohaemagglutinin-stimulated human peripheral blood mononuclear cells and virtual screening. *Journal of Ethnopharmacology* 2018; **226**, 44-47.

[33] C Frezza, A Venditti, DD Vita, C Toniolo, M Franceschin, A Ventrone, L Tomassini , S Foddai, M Guiso, M Nicoletti, A Bianco, M Serafini. Phytochemistry, chemotaxonomy and biological activities of the Araucariaceae family—a review. *Plants* 2020; **9(7)**, 888.

[34] Kurniawanti, DD Agusta, P Sugita, IH Suparto, H Dianhar and DUC Rahayu. Bioactive compounds of flavone dimers from Indonesian *Araucaria columnaris* leaves. *Rasayan Journal of Chemistry* 2023; **16(3)**, 1872-1882.

[35] P Sugita, SDP Handayani, DD Agusta, L Ambarsari, H Dianhar and DUC Rahayu. Combined *in-silico* and *in-vitro* approaches to evaluate the inhibitory potential of biflavonoids from *Araucaria* plants against α-glucosidase as target protein. *Rasayan Journal of Chemistry* 2023; **16(1)**, 361-375

[36] SS El-Hawary, MA Rabeh, MAE Raey, EMA El-Kadder, M Sobeh, UR Abdelmohsen, A Albohy, AM Andrianov, IP Bosko, MM Al-Sanea and DG El-Kolobby. Metabolomic profiling of three Araucaria species and their possible potential role against COVID-19. *Journal of Biomolecular Structure and Dynamics* 2021; **40(14)**, 6426-6438.

[37] L Irfana, DD Agusta, B Arifin, ST Wahyudi, SS Achmadi and P Sugita. Biflavonoid from Indonesian Araucaria cunninghamii Mudie leaves activity against breast cancer and 20s proteasome. *Trends in Sciences* 2025; **22(3)**, 9198.

[38] K Ramayanti, H Riza and I Fajriaty. Molecular docking of drymaritin, tiptonine A and triptonine B compounds against HIV enzymes. *Jurnal Mahasiswa Farmasi Fakultas Kedokteran UNTAN* 2019; **1**, 1-6.

[39] VTT Le, HV Hung, NX Ha, CH Le, PTH Minh and DT Lam. Natural phosphodiesterase-4 inhibitors with potential anti-inflammatory activities from *Millettia dielsiana*. *Molecules* 2023; **28(21)**, 7253.

[40] F Awaluddin, I Batubara and ST Wahyudi. Molecular dynamics simulation of bioactive compounds against six protein targets of SARS-CoV-2 as COVID-19 antivirus candidates. *Jurnal Kimia Valensi* 2021; **7(2)**, 178-187.

[41] T Hou, J Wang, Y Li and W Wang. Assessing the performance of the MM/PBSA and MM/GBSA methods: The accuracy of binding free energy calculations based on molecular dynamics simulations. *Journal of Chemical Information and Modeling* 2011; **51(1)**, 69-82.

[42] M Sasikala, R Sundaraganapathy and S Mohan. MTT assay on anticancer properties of phytoconstituents from Ipomoea aquatica Forssk. using MCF–7 cell lines for breast cancer in women. *Research Journal of Pharmacy and Technology* 2020; **13(3)**, 1356-1360.

[43] J Cheng, Y Li and J Kong. Ginkgetin inhibits proliferation of HeLa cells via activation of p38/NF-κB pathway. *Cellular and Molecular Biology* 2019; **65(4)**, 79-82.

[44] M Luthfia, A Eryandini, D Geraldi, C Narita, CM Jannah and L Ambarsari. Potency of bioactive compounds in Indramayu mango peel waste to inhibit ACE2. *Current Biochemistry* 2021; **8(2)**, 51-62.

[45] MZS Al-Khayyat and AGA Al-Dabbagh. *In silico* prediction and docking of tertiary structure of LuxI, an inducer synthase of vibrio fischeri. *Reports of Biochemistry and Molecular Biology* 2016; **4(2)**, 66-75.

[46] K Anwar, E Suhartono and N Komari. Three dimension structure modeling of the superoxide dismutase (SOD) of rice (*Oryza sativa*) using fold recognition method using Phyre2 web server. *Jurnal Ilmiah Berkala Sains dan Terapan Kimia*

2022; **16(2)**, 86-97.

[47] Nafisah, Sarmila, H Habibah, I Saputri, I Setiawati and N Komari. Effect of Kelakai (*Stenochlaena palustris*) extract on organophosphate pesticide exposure: Cytotoxic studies *in silico* and in ovo. *Jurnal Ilmiah Berkala Sains dan Terapan Kimia* 2023; **17(2)**, 1-14.

[48] R Vaidyanathan, SM Sreedevi, K Ravichandran, SM Vinod, YH Krishnan, LH Babu, PS Parthiban, L Basker, T Perumal, V Rajaraman, G Arumugam, K Rajendran and V Mahalingam. Molecular docking approach on the binding stability of derivatives of phenolic acids (DPAs) with human serum albumin (HSA): Hydrogen-bonding versus hydrophobic interactions or combined influences?. *Journal of Colloid and Interface Science Open* 2023; **12**, 100096.

[49] S Genheden and U Ryde. The MM/PBSA and MM/GBSA methods to estimate ligand-binding affinities. *Expert Opinion on Drug Discovery* 2015; **10(5)**, 449-461.

[50] GJ Kim, EJ Yang, YS Kim, J Moon, YK Son, JW Nam, I Choi, H Choi and KS Song. Diterpene and biflavone derivatives from Thuja koraiensis and their cytotoxicities against A549 cells. *Phytochemistry* 2023; **211**, 113711.

[51] LS Sreeshma and BR Nair. A simple protocol for the isolation of amentoflavone from two species of Biophytum DC. (Oxalidaceae) and evaluation of its antiproliferative potential. *Industrial Crops and Products* 2021; **160**, 113099.

[52] CAD Lima, LK Maquedano, LS Jaalouk, DCD Santos and GB Longato. Biflavonoids: Preliminary reports on their role in prostate and breast cancer therapy. *Pharmaceuticals* 2024; **17(7)**, 874.

[53] AG Mercader and AB Pomilio. Naturally-occurring dimers of flavonoids as anticarcinogens. *Anti-Cancer Agents in Medicinal Chemistry* 2013; **13(8)**,1217-1235.

[54] M Drees, R Zimmermann and G Eisenbrand. 3',5'-Cyclic nucleotide phosphodiesterase in tumor cells as potential target for tumor growth inhibition. *Cancer Research*1993; **53(13)**, 3058-3061.

[55] SJ MacKenzie and MD Houslay. Action of rolipram on specific PDE4 cAMP phosphodiesterase isoforms and on the phosphorylation of cAMP-response-element-binding protein (CREB) and p38 MAP kinase in U937 monocytic cells. *Biochemical Journal* 2000; **347(2)**, 571-578.

[56] R Yuniarti, S Nadia, A Alamanda, M Zubir, RA Syahputra and M Nizam. Characterization, phytochemical screenings and antioxidant activity test of Kratom leaf ethanol extract (*Mitragyna speciosa* Korth) using DPPH method. *Journal of Physics: Conference Series* 2020; **1462**, 012026.

[57] MM Alanazi, E Alaa, NA Alsaif, AJ Obaidullah, HM Alkahtani, AA Al-Mehizia, SM Alsubaie, MS Taghour and IH Eissa. Discovery of new 3-methylquinoxalines as potential anti-cancer agents and apoptosis inducers targeting VEGFR-2: design, synthesis and *in silico* studies. *Journal of Enzyme Inhibition and Medicinal Chemistry* 2021; **36(1)**, 1732-1750.

[58] Y Yu, Y Zhao, Y Wang and X Huang. Design and synthesis of novel PDE4 inhibitors as potential candidates for antidepressant agents. *Journal of Chemical Research* 2023. https://doi.org/10.1177/17475198231202967

[59] YN Liu, YY Huang, JM Bao, YH Cai, YQ Guo, SN Liu, HB Luo and S Yin. Natural phosphodiesterase-4 (PDE4) inhibitors from *Crotalaria ferruginea*. *Fitoterapia* 2014; **94**, 177-182.

[60] CY Teo, KM Loh, JF Chai, HX Wang, RP Tan, SW Ho and LP Lim. Discovery of a new class of inhibitors for the protein arginine deiminase type 4 (PAD4) by structure-based virtual screening. *BMC Bioinformatics* 2012; **13(S17)**, S4.

[61] X Zhang L Jin, Y Wu, B Huang, K Chen, W Huang and J Li. Anti-inflammatory properties of biflavonoids derived from Selaginella moellendorffii Hieron: Targeting NLRP3 inflammasome-dependent pyroptosis. *Journal of Ethnopharmacology* 2025; **340**, 119172.

Supplementary Material

Detailed information of the AutoDock Vina command-line input and configuration files in Data of *In Silico*

Table S1 Overall affinity value (kcal/mol) from cross docking results of PDE4B and PDE4D towards test and comparison ligands.

Protein	Ligand	Binding affinity (kcal/mol)										
		1TB5	**2CHM**	**1XMU**	**2QYL**	**4KP6**	**4MYQ**	**4NW7**	**5OHJ**	**1XN0**	**3WD9**	**Mean ± SD**
PDE4B	**13**	-10.81	-11.13	-11.42	-11.03	-10.95	-10.11	-10.62	-10.99	-10.52	-11.56	-10.90 ± 0.41
	12	-10.72	-11.47	-10.52	-10.30	-10.55	-8.63	-11.45	-10.26	-10.45	-12.31	-10.71 ± 1.07
	11	-10.76	-10.58	-10.08	-10.05	-10.68	-10.18	-10.02	-9.87	-10.24	-13.24	-10.57 ± 1.00
	15	-9.53	-10.33	-10.06	-9.51	-10.83	-10.73	-10.93	-10.41	-10.26	-12.76	-10.54 ± 0.94
	9	-9.46	-10.30	-10.24	-9.32	-10.29	-10.53	-10.73	-10.70	-10.33	-11.40	-10.35 ± 0.65
	10	-9.97	-9.44	-10.44	-10.20	-11.16	-7.60	-8.87	-10.32	-10.05	-12.84	-10.09 ± 1.38
	24	-9.13	-10.50	-9.58	-9.82	-9.69	-10.80	-9.07	-11.00	-11.35	-10.11	-10.09 ± 0.98
	14	-10.62	-10.18	-9.81	-9.98	-10.58	-8.63	-9.02	-9.80	-9.74	-12.10	-9.98 ± 0.82
	23	-9.90	-9.29	-9.70	-10.67	-9.49	-10.75	-9.86	-10.71	-10.05	-8.74	-9.85 ± 0.81
	01	-9.76	-8.96	-11.37	-10.46	-10.20	-8.07	-9.86	-10.07	-9.89	-9.91	-9.80 ± 1.39
	04	-10.28	-9.82	-10.74	-9.77	-9.60	-7.50	-7.47	-10.61	-10.32	-11.68	-9.64 ± 1.09
	2	-10.27	-9.04	-9.75	-9.78	-10.61	-8.75	-8.32	-10.28	-8.83	-10.08	-9.54 ± 0.76
	16	-9.04	-8.29	-8.08	-10.00	-10.86	-7.49	-11.41	-9.57	-9.48	-10.95	-9.50 ± 1.43
	3	-9.72	-9.31	-10.51	-9.80	-9.93	-6.40	-7.76	-10.52	-9.84	-10.92	-9.50 ± 0.88
	8	-10.15	-9.71	-10.02	-9.74	-9.59	-9.24	-7.47	-10.08	-8.59	-10.09	-9.28 ± 1.24
	5	-9.48	-8.92	-10.43	-9.59	-9.74	-6.53	-7.98	-9.50	-8.82	-9.85	-9.06 ± 1.10
	7	-9.92	-9.05	-10.13	-9.39	-9.84	-6.57	-5.82	-10.24	-8.89	-8.41	-8.64 ± 1.68
	6	-9.69	-9.23	-9.91	-9.52	-9.29	-5.51	-5.15	-10.26	-9.13	-7.95	-8.54 ± 1.82
	25	-8.56	-9.24	-8.30	-10.00	-8.71	-9.56	-4.39	-9.73	-9.94	-6.04	-8.54 ± 1.75
	22	-7.81	-7.26	-7.29	-7.99	-10.71	-5.95	-11.17	-9.58	-6.53	-8.16	-8.23 ± 1.73
	19	-8.72	-8.00	-9.79	-7.96	-8.90	-2.42	-6.31	-8.78	-8.75	-9.39	-7.92 ± 2.16
	17	-7.71	-8.82	-7.19	-9.23	-10.78	-0.54	-5.65	-9.84	-8.04	-7.20	-7.44 ± 2.87
	18	-8.55	-8.92	-8.83	-9.69	-10.21	-0.71	-3.24	-9.97	-7.53	-6.50	-7.39 ± 3.14
	21	-8.79	-7.32	-7.50	-8.65	-8.23	-2.59	-3.88	-9.40	-6.01	-8.28	-7.06 ± 2.24
	20	-8.00	-8.44	-7.61	-8.15	-9.85	-1.68	-2.66	-9.58	-6.46	-7.49	-6.99 ± 2.73
	CMP	-7.80	-7.42	-8.95	-8.16	-7.05	-8.15	-8.54	-8.16	-7.74	-7.68	-7.95 ± 0.55

Protein	Ligand	Binding affinity (kcal/mol)										
		1TB5	**2CHM**	**1XMU**	**2QYL**	**4KP6**	**4MYQ**	**4NW7**	**5OHJ**	**1XN0**	**3WD9**	**Mean ± SD**
	ROF	-7.78	-8.12	-9.00	-9.03	-8.05	-8.99	-8.82	-8.84	-9.33	-8.66	-8.67 ± 0.51
	ROL	-7.04	-7.18	-7.68	-8.14	-7.89	-8.37	-6.91	-7.98	-8.18	-7.86	-7.74 ± 0.53
		1OYN	**1XOQ**	**1Y2B**	**6FDC**	**6IMD**	**6IMI**	**6IMT**	**6LRM**	**7B9H**	**7CBJ**	**Mean ± SD**
PDE4D	**24**	-9.96	-10.45	-10.17	-11.01	-9.78	-9.92	-10.93	-9.83	-10.86	-10.20	-10.30 ± 0.48
	15	-10.20	-10.48	-10.37	-10.26	-10.19	-10.59	-10.99	-9.95	-10.01	-9.70	-10.27 ± 0.36
	13	-11.02	-10.62	-10.09	-9.94	-10.30	-10.31	-10.25	-9.99	-10.23	-9.60	-10.24 ± 0.39
	23	-9.90	-10.63	-9.55	-11.37	-9.79	-9.72	-10.19	-10.44	-10.97	-9.64	-10.22 ± 0.62
	12	-10.44	-10.22	-10.17	-10.26	-10.58	-10.56	-10.61	-9.42	-10.16	-9.59	-10.20 ± 0.41
	11	-9.89	-10.30	-10.08	-10.66	-10.07	-9.83	-10.38	-10.12	-10.56	-9.68	-10.17 ± 0.31
	04	-10.92	-10.50	-9.84	-10.07	-9.96	-9.37	-9.88	-9.51	-11.25	-9.35	-10.06 ± 0.60
	16	-10.02	-9.78	-10.08	-10.40	-10.06	-10.68	-10.54	-10.42	-10.05	-8.53	-10.05 ± 0.34
	10	-10.12	-10.20	-10.07	-9.99	-10.30	-10.48	-10.18	-9.71	-10.02	-9.30	-10.04 ± 0.33
	09	-10.63	-9.88	-9.76	-10.06	-10.26	-10.19	-10.18	-9.68	-9.70	-9.56	-9.99 ± 0.34
	22	-9.73	-9.97	-10.27	-9.71	-10.56	-10.45	-10.45	-9.47	-9.95	-8.76	-9.93 ± 0.55
	01	-10.19	-10.67	-8.57	-10.01	-9.33	-9.23	-10.40	-9.79	-10.43	-10.12	-9.88 ± 0.65
	14	-9.87	-10.29	-9.77	-10.74	-9.54	-9.35	-9.35	-9.78	-10.47	-9.54	-9.87 ± 0.48
	02	-9.35	-9.89	-9.87	-9.56	-10.72	-10.59	-10.23	-9.43	-9.25	-9.47	-9.84 ± 0.52
	08	-9.39	-10.29	-9.08	-9.83	-9.46	-9.20	-9.63	-9.82	-9.93	-9.65	-9.62 ± 0.36
	17	-8.94	-9.46	-9.36	-9.60	-10.11	-9.87	-10.05	-8.78	-9.95	-8.63	-9.46 ± 0.56
	18	-8.97	-9.63	-9.49	-9.69	-9.74	-9.48	-9.45	-9.32	-9.40	-8.75	-9.39 ± 0.32
	3	-9.83	-9.86	-8.94	-10.13	-8.62	-8.69	-9.33	-9.05	-9.97	-9.21	-9.36 ± 0.55
	6	-9.26	-9.78	-8.60	-10.45	-9.12	-8.89	-9.12	-8.72	-10.06	-8.91	-9.29 ± 0.61
	7	-9.14	-9.90	-8.77	-9.63	-8.48	-8.54	-9.56	-9.32	-9.83	-9.37	-9.26 ± 0.51
	5	-8.82	-9.72	-8.92	-9.48	-8.72	-9.07	-9.37	-9.30	-9.29	-9.78	-9.25 ± 0.36
	25	-8.97	-9.45	-8.39	-9.43	-9.01	-9.05	-9.13	-8.92	-10.05	-9.75	-9.23 ± 0.46
	20	-8.56	-8.65	-8.71	-8.09	-9.51	-9.05	-9.57	-7.39	-8.92	-7.19	-8.56 ± 0.80
	19	-8.46	-9.28	-8.02	-9.02	-7.30	-7.41	-7.81	-8.55	-8.22	-7.73	-8.19 ± 0.66
	21	-7.97	-7.81	-7.65	-8.12	-8.43	-8.35	-8.41	-7.75	-8.40	-8.03	-8.10 ± 0.29
	CMP	-8.29	-8.62	-8.43	-7.47	-8.31	-8.05	-8.63	-6.98	-7.98	-6.73	-7.95 ± 0.67
	ROF	-8.48	-8.54	-8.35	-8.59	-8.42	-8.34	-8.29	-7.92	-8.55	-7.71	-8.32 ± 0.29
	ROL	-8.31	-8.57	-7.87	-7.46	-7.83	-7.69	-7.67	-6.62	-8.22	-6.76	-7.70 ± 0.63

PDE4B

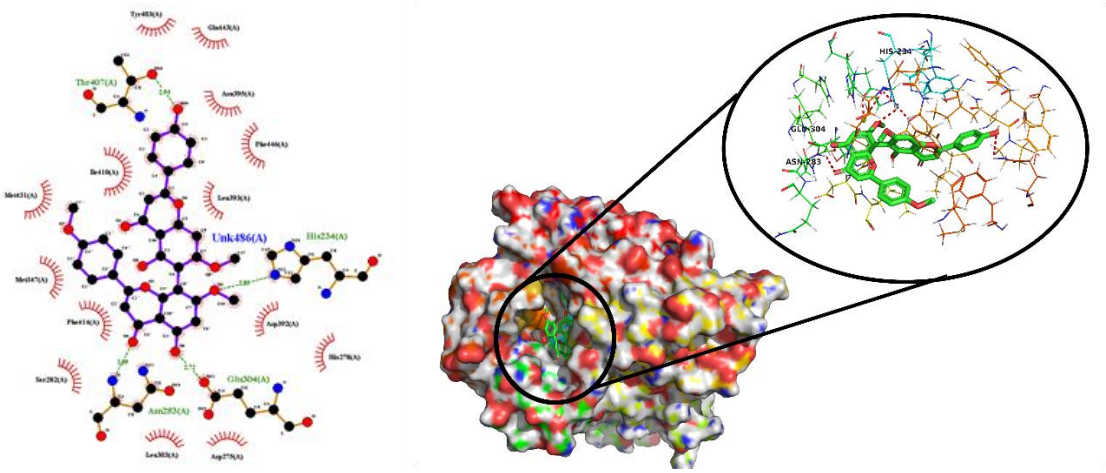

Compound 5

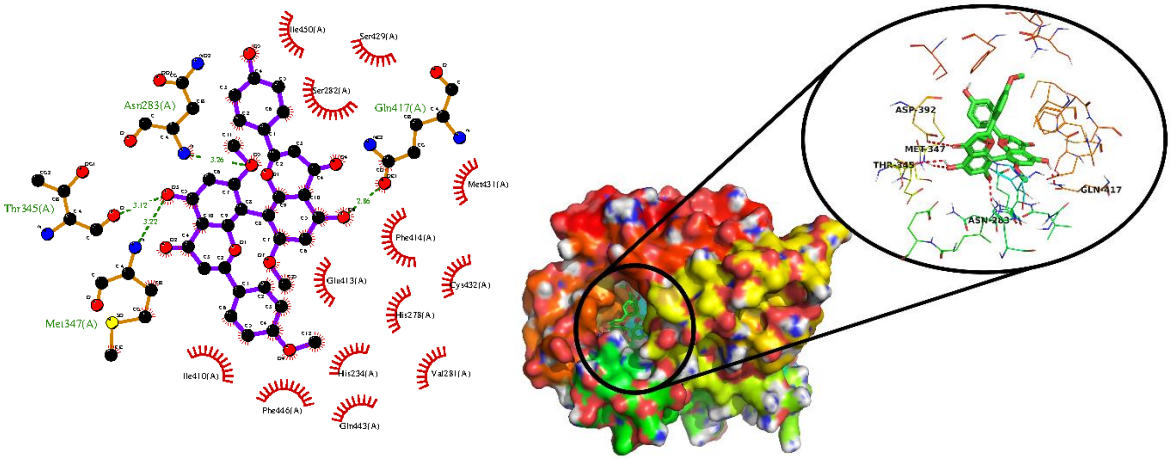

Compound 18

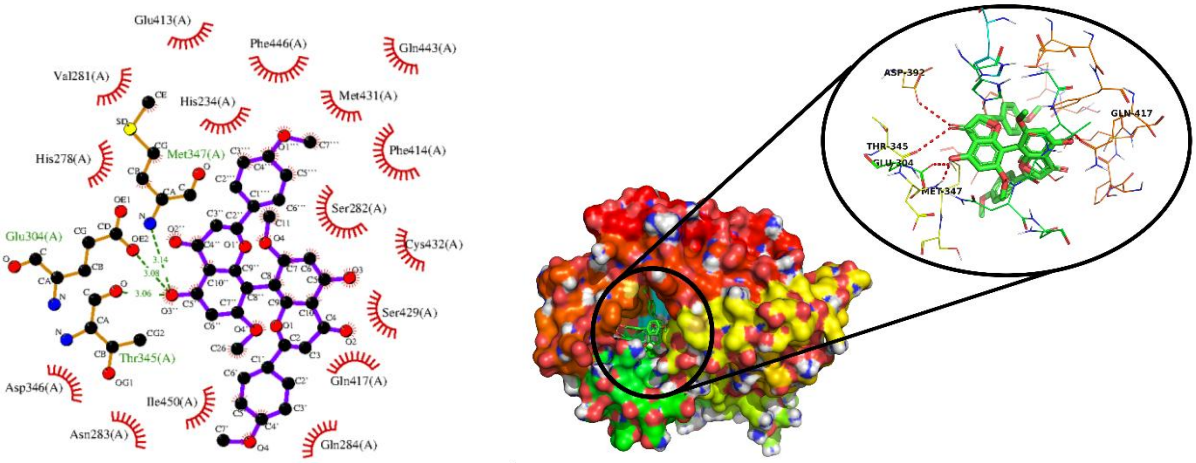

Compound 20

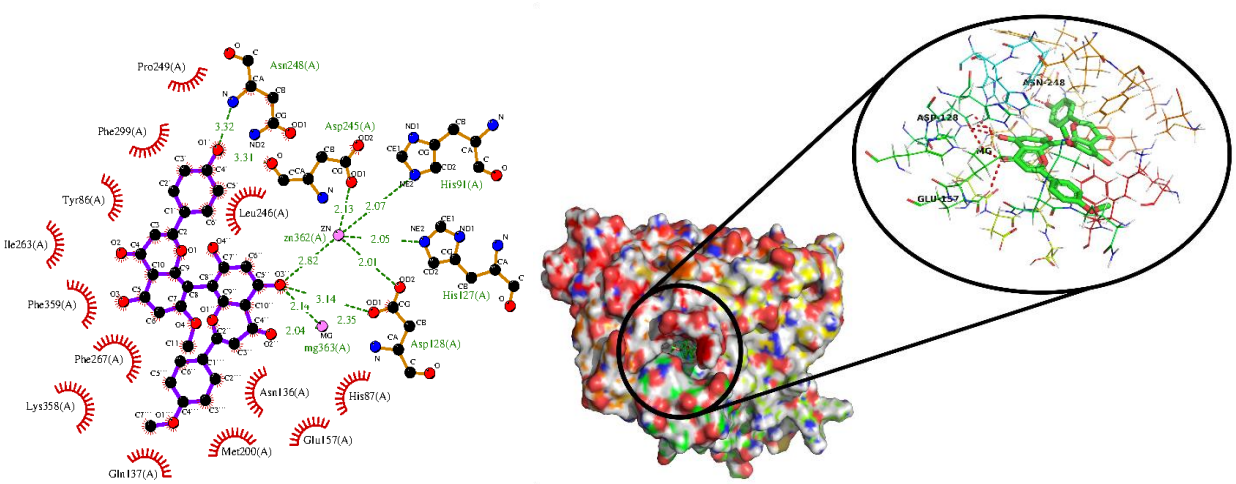

Compound 22

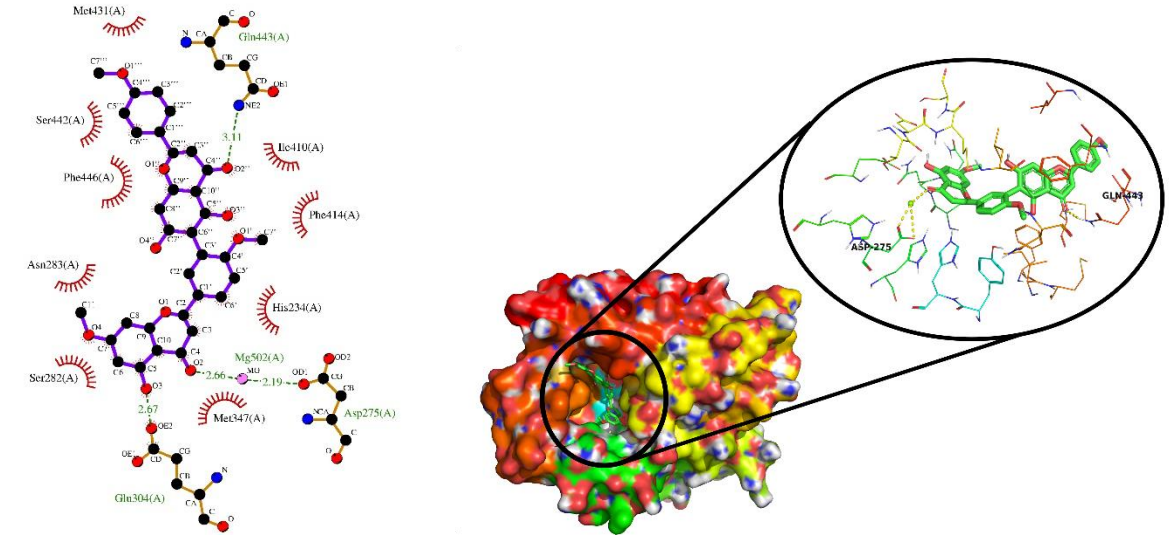

Compound 25

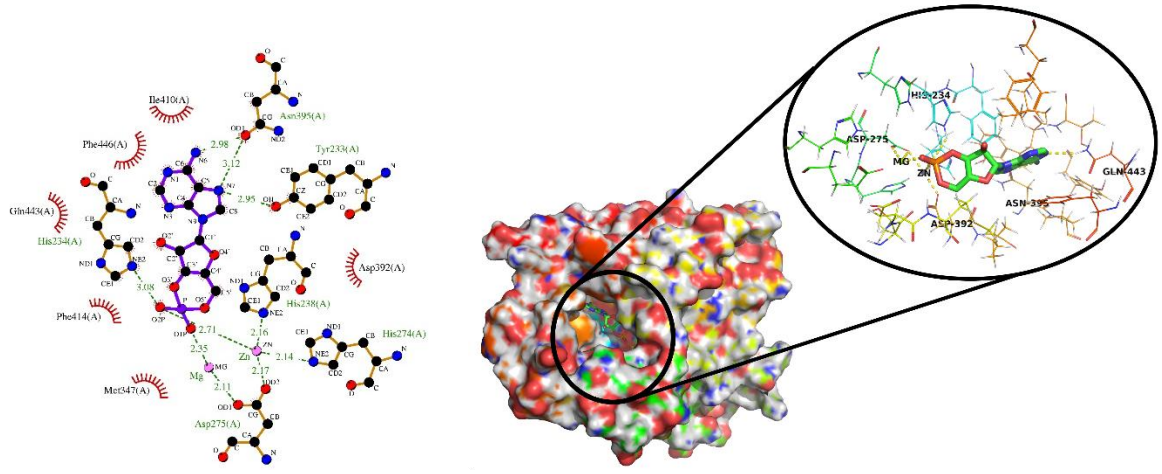

Compound c-AMP (CMP)

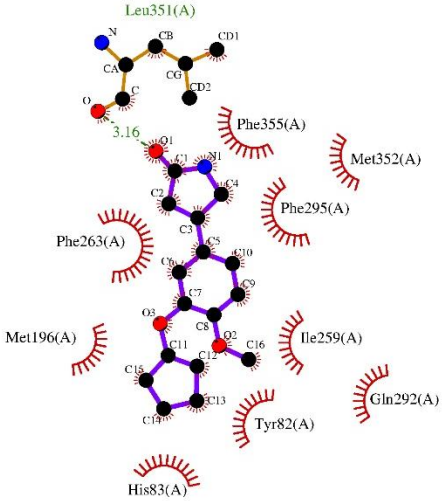

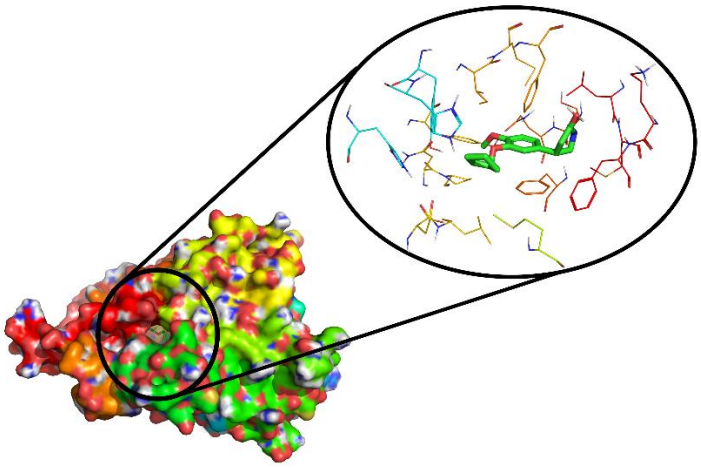

Compound ROL

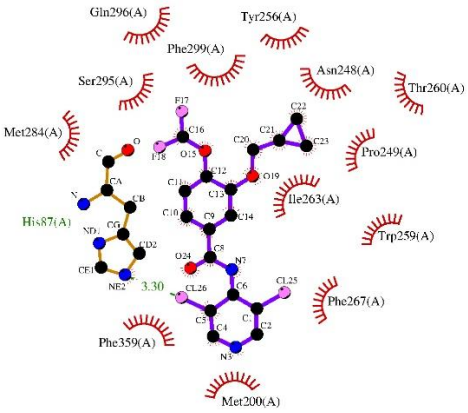

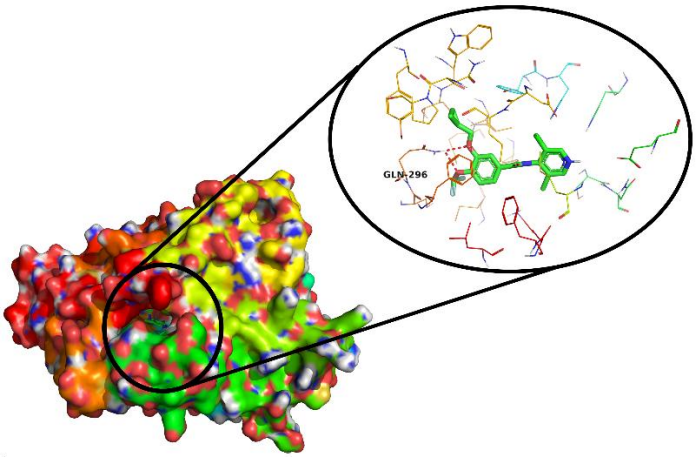

Compound ROF

PDE4D

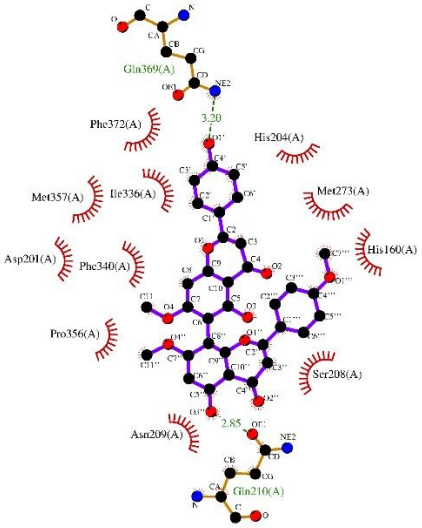

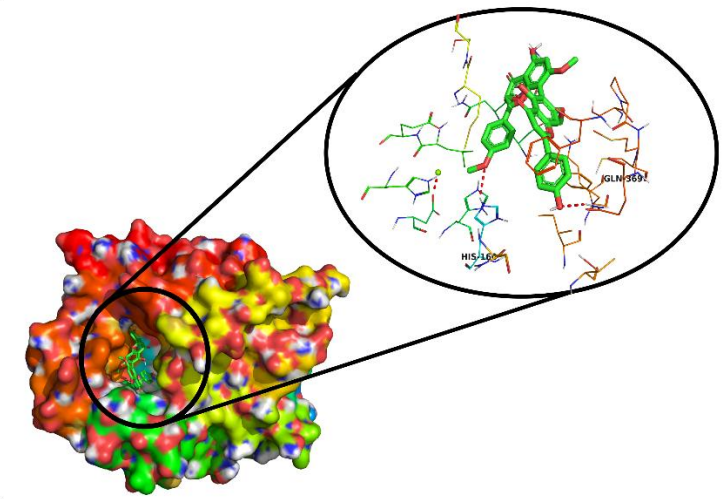

Compound 5

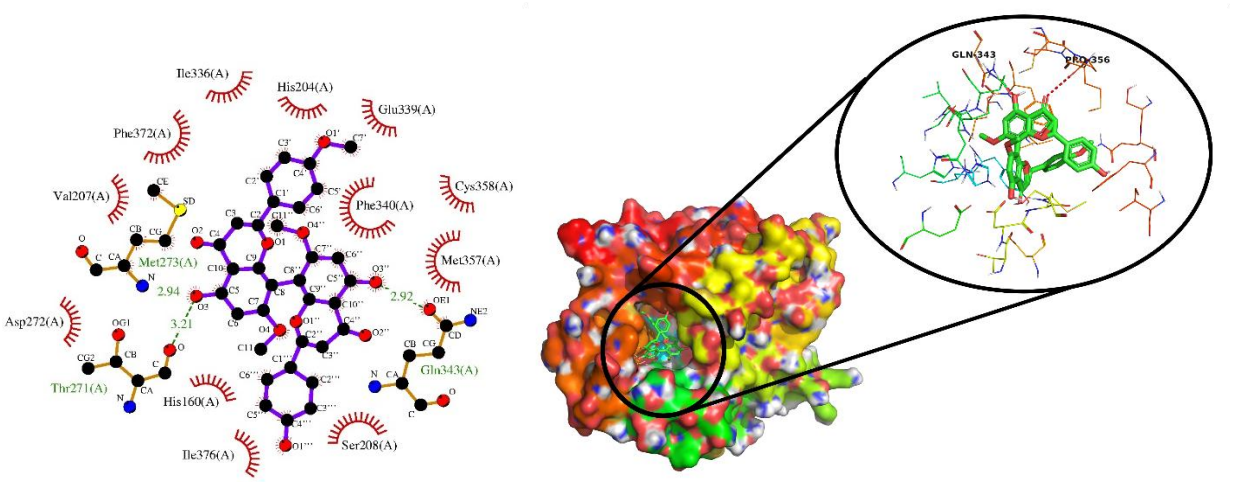

Compound 18

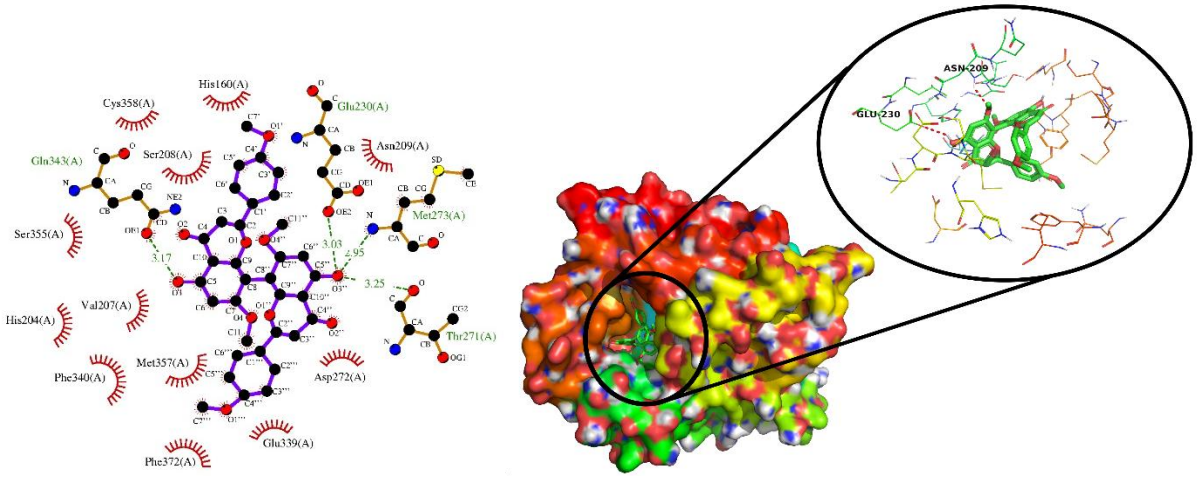

Compound 20

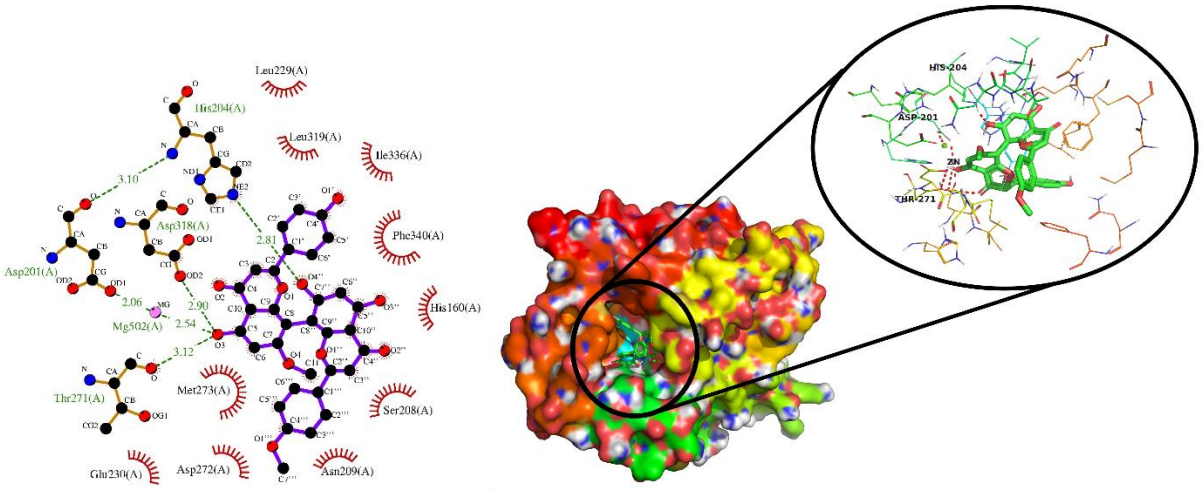

Compound 22

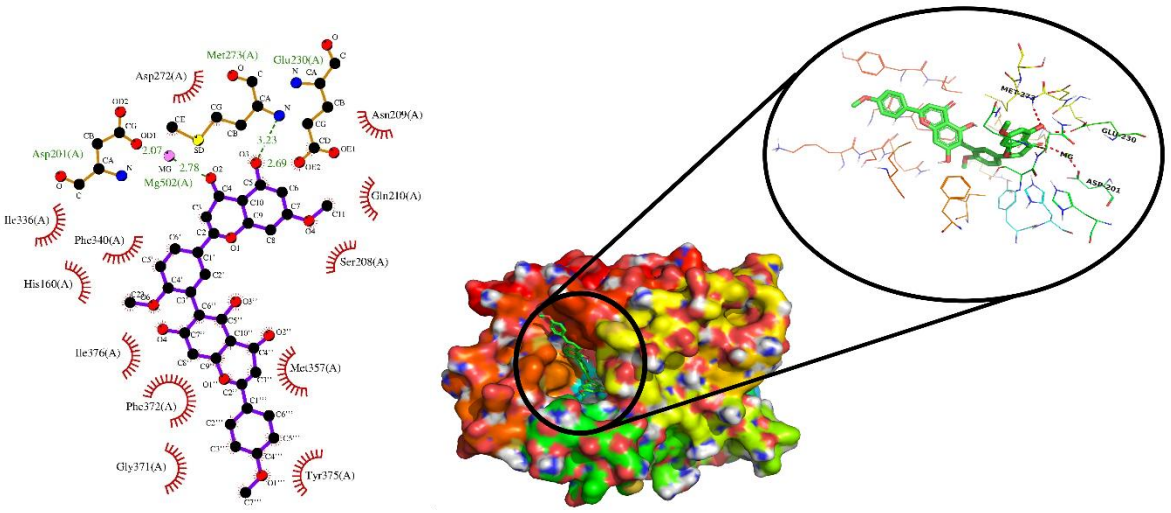

Compound 25

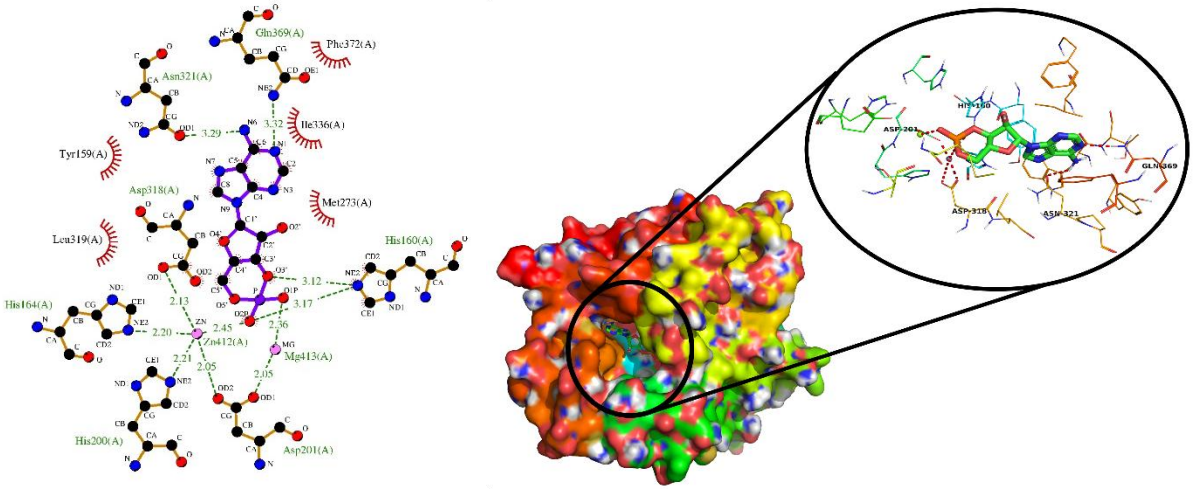

Compound C-AMP/CMP

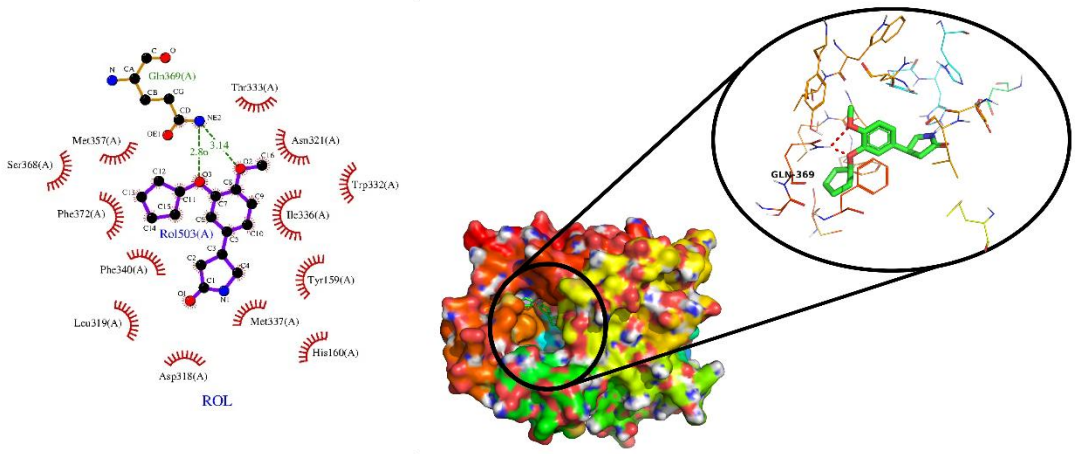

Compound ROL

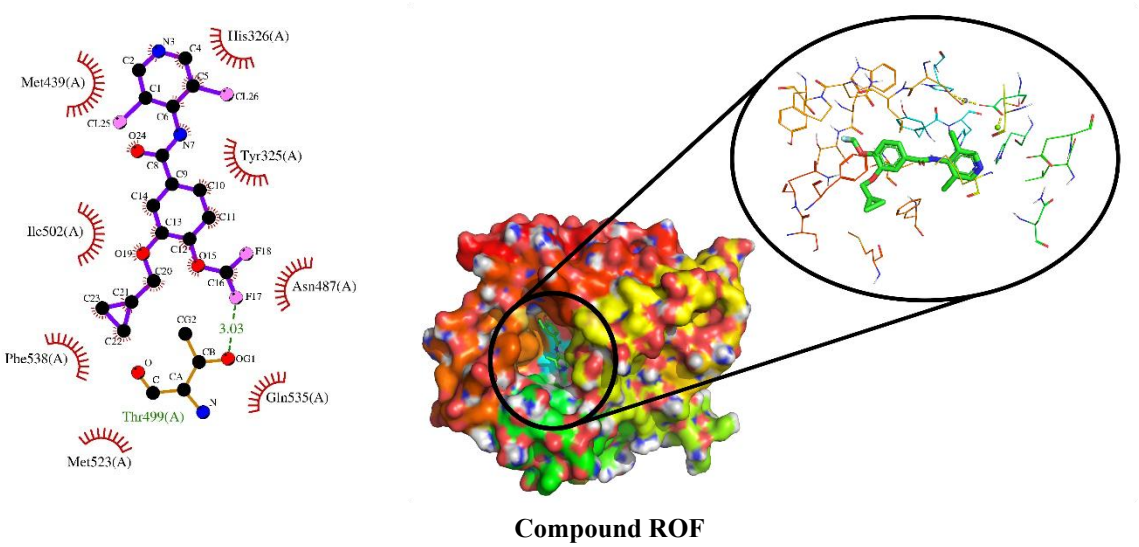

Figure S1 2D and 3D visualization of binding of test compounds (except compound **13**) and comparison ligands to PDE4B and PDE4D proteins.

Table S2 Calculation data for the inhibitory activity of PDE4B and PDE4D enzymes.

Enzyme	Compound	Consentration (µM)	Absorbance		% Inhibition		Mean % Inhibition	SD % Inhibition	IC_{50} (µM)		Mean IC_{50} (µM)	SD IC_{50} (µM)
			R1	R2	R1	R2			R1	R2		
PDE4B	**5**	Control	0.122	0.107	0.00	0.00	0.00	0.00	843.30	817	830.15	13.15
		250	0.094	0.081	22.95	24.30	23.63	0.95				
		500	0.071	0.057	41.80	46.73	44.27	3.49				
	13	Control	0.122	0.107	0.00	0.00	0.00	0.00	16.28	11.52	13.9	2.38
		0.5	0.125	0.107	-2.46	0.00	-1.23	1.74				
		1.5	0.098	0.080	19.67	25.23	22.45	3.93				
		6.25	0.091	0.077	25.41	28.04	26.73	1.86				
		12.5	0.075	0.072	38.52	32.71	35.62	4.11				
		25	0.021	0.034	82.79	68.22	75.51	10.30				
	18	Control	0.122	0.107	0.00	0.00	0.00	0.00	445.10	457.8	451.45	6.35
		250	0.066	0.055	45.90	48.60	47.25	1.91				
		500	0.072	0.070	40.98	34.58	37.78	4.53				
	20	Control	0.122	0.121	0.00	0.00	0.00	0.00	1356	1358	1357	1
		125	0.120	0.131	1.64	-8.26	-3.31	7.00				
		250	0.108	0.119	11.48	1.65	6.56	6.95				
		500	0.098	0.118	19.67	2.48	11.08	12.16				
		800	0.093	0.103	23.77	14.88	19.32	6.29				
		1000	0.036	0.027	70.49	77.69	74.09	5.09				

Enzyme	Compound	Consentration (µM)	Absorbance		% Inhibition		Mean % Inhibition	SD % Inhibition	IC_{50} (µM)		Mean IC_{50} (µM)	SD IC_{50} (µM)
			R1	R2	R1	R2			R1	R2		
PDE4D	**22**	Control	0.122	0.107	0.00	0.00	0.00	0.00	129	114,4	121.70	7.30
		31,25	0.090	0.079	26.23	26.17	26.20	0.04				
		62,50	0.088	0.073	27.87	31.78	29.83	2.76				
	25	Control	0.122	0.107	0.00	0.00	0.00	0.00	231.40	218.8	225.10	6.30
		62,5	0.106	0.112	13.11	-4.67	4.22	8.89				
		125	0.103	0.080	15.57	25.23	20.40	4.83				
		250	0.056	0.023	54.10	78.50	66.30	12.20				
		500	0.077	0.094	36.89	12.15	24.52	12.37				
		800	0.106	0.125	13.11	-16.82	-1.86	14.97				
	5	Control	0.156	0.164	0.00	0.00	0.00	0.00	861.3	831.9	846.6	14.70
		250	0.144	0.104	7.69	36.59	22.14	14.45				
		500	0.111	0.087	28.85	46.95	37.90	9.05				
	13	Control	0.156	0.164	0.00	0.00	0.00	0.00	18.52	11.52	15.02	3.50
		0.5	0.142	0.107	8.97	34.76	21.87	12.90				
		1.5	0.144	0.080	7.69	51.22	29.46	21.77				
		6.25	0.127	0.077	18.59	53.05	35.82	17.23				
		12.5	0.108	0.072	30.77	56.10	43.44	12.67				
		25	0.079	0.034	49.36	79.27	64.32	14.96				
	18	Control	0.156	0.164	0.00	0.00	0.00	0.00	429	560.6	494.8	65.8
		250	0.101	0.072	35.26	56.10	45.68	10.42				
		500	0.121	0.086	22.44	47.56	35.00	12.56				
	20	Control	0.156	0.164	0.00	0.00	0.00	0.00	1347	1211	1279	68
		125	0.133	0.189	14.74	-15.24	-0.25	14.99				
		250	0.141	0.156	9.62	4.88	7.25	2.37				
		500	0.140	0.161	10.26	1.83	6.05	4.22				
		800	0.096	0.130	38.46	20.73	29.60	8.87				
		1000	0.046	0.061	70.51	62.80	66.66	3.86				
	22	Control	0.156	0.164	0.00	0.00	0.00	0.00	127.3	132.7	130	2.7
		31,25	0.148	0.104	5.13	36.59	20.86	15.73				
		62,50	0.135	0.103	13.46	37.20	25.33	11.87				
	25	Control	0.156	0.164	0.00	0.00	0.00	0.00	219.9	217.2	218.55	1.35
		62,5	0.120	0.162	23.08	1.22	12.15	10.93				
		125	0.111	0.126	28.85	23.17	26.01	2.84				
		250	0.042	0.039	73.08	76.22	74.65	1.57				
		500	0.130	0.116	16.67	29.27	22.97	6.30				
		800	0.172	0.172	-10.26	-4.88	-7.57	2.69				

Note: Repetition 1 (R1) and standar deviation (SD).

Sample calculation example (Compound **13** - 25 ppm);

$$\%\ Inhibition = \frac{Absorbance_{control} - Absorbance_{sample}}{Absorbance_{control}} \times 100\%$$

$$\%\ Inhibition = \frac{0{,}122 - 0.021}{0{,}122} \times 100\%$$

$$\%\ Inhibition = 82{,}79\ \%$$

Graph of the non-linear regression equation between % inhibition and concentration and IC_{50} value produced in replication 1 of compound **13** for the PDE4B enzyme.

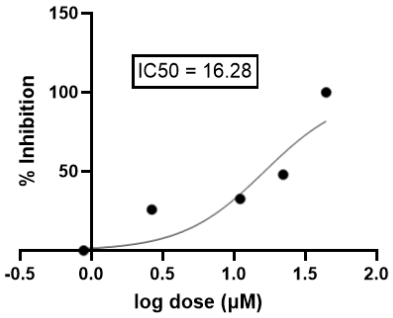

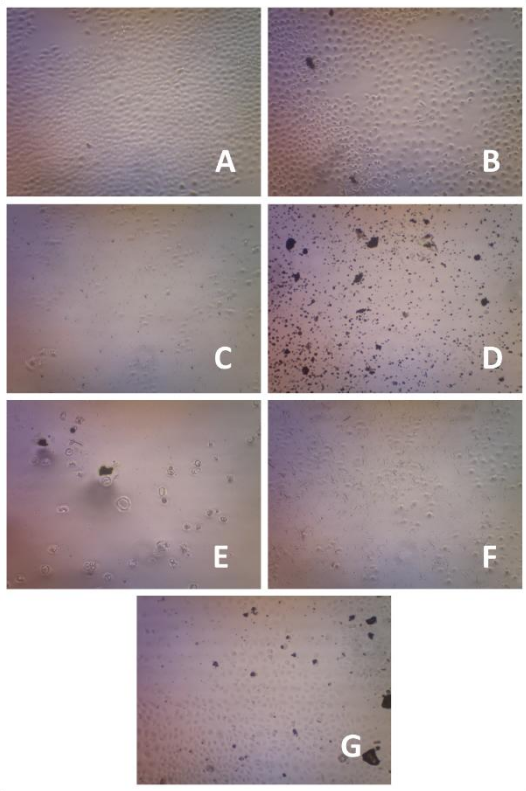

Figure S2 Microscope observation at 400× magnification of untreated (negative control, (A) and treated (25 ppm of compound **13** (B), 62.5 ppm of compound **22** (C) and 250 ppm of compound **25** (D), **18** (E), **5** (F), **20** (G)) MCF-7 cell samples.